Heliyon 10 (2024) e39068

Contents lists available at ScienceDirect

Heliyon

journal homepage: www.cell.com/heliyon

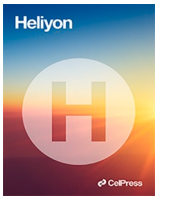

Research article

Elucidating the dynamics of carbamazepine uptake using date pit-derived activated carbon: A comprehensive kinetic and thermodynamic analysis

Ramez M. Zayyat [a,*], Rim Yahfoufi [b], Mahmoud Al-Hindi [b,**], Michel A. Kordahi [a], George M. Ayoub [a], Mohammad N. Ahmad [b]

[a] Department of Civil and Environmental Engineering, American University of Beirut, P.O. Box 11-0236, Riad El Solh, Beirut, 1107 2020, Lebanon
[b] Department of Chemical Engineering and Advanced Energy, American University of Beirut, P.O. Box 11-0236, Riad El Solh, Beirut, 1107 2020, Lebanon

ARTICLE INFO

Keywords:
Phenomenological modeling
Date pits
Activated bio-waste material
Low-cost adsorbent
Carbamazepine
Linear driving force

ABSTRACT

Water contamination with pharmaceuticals such as Carbamazepine (CBZ) presents a significant environmental challenge. This study investigates the use of activated carbon derived from waste date pits (DPAC) for the removal of CBZ from water. The impact of several parameters such as pH, temperature, CBZ concentration, and flow rate on the adsorption were assessed. The generated DPAC demonstrated a specific surface area of 309 m^2/g, a pore volume of 0.264 cm^3/g, and the pores are mainly distributed at 1.86, 2.73, and 3.43 nm. The Langmuir, Freundlich, Sips, and Toth isotherms were used to fit the experimental data, and the results indicate the occurrence of monolayer adsorption and heterogeneous surface conditions. The Linear Driving Force model was used for kinetic analysis, showing improved fit at higher concentrations. Thermodynamic analyses revealed the process to be endothermic, spontaneous, and entropically driven. The DPAC achieved an adsorption capacity of 14.89 mg/g and maintained 94 % effectiveness after the first regeneration cycle and 70 % after four cycles. This study highlights the potential of DPAC as a sustainable adsorbent for advanced water purification.

1. Introduction

The occurrence of pharmaceuticals in water bodies and their impact on the environment has received considerable attention over the last two decades [1]. Although pharmaceutically active compounds are designed to exhibit low half-lives, they are persistent even after wastewater treatment [1,2]. Pharmaceuticals find their way into natural waters as result of several aspects of human activity [1,2] as well as the improper disposal of expired drugs [3]. One of the most commonly detected pharmaceuticals in water bodies is CBZ, which is used to treat epilepsy in humans and animals as well as bipolar disorders. It is used worldwide and has been recognized as one of the most significant priority pharmaceuticals in several regions in the world [4] as it exhibits a low removal efficiency in sewage treatment plants and is highly persistent in the aquatic environment [5]. Its low degradability gives CBZ its title as a persistent organic pollutant (POP). Samples have shown that CBZ is present in most natural waterways including freshwater, seawater, and groundwater

* Corresponding author.
** Corresponding author.
E-mail addresses: rz29@aub.edu.lb (R.M. Zayyat), ma211@aub.edu.lb (M. Al-Hindi).

https://doi.org/10.1016/j.heliyon.2024.e39068
Received 6 March 2024; Received in revised form 13 September 2024; Accepted 7 October 2024
Available online 10 October 2024

thus proving the low degradability of this compound [1]. According to Kahle et al. [6] the concentrations of CBZ in natural waters and wastewater treatment plants (WWTPs) can range from 0.14 μg/L to several micrograms per liter. The authors detected CBZ levels between 2 and 70 ng/L in lakes, and up to 42 ng/L in ground water aquifers influenced by wastewater discharges from WWTPs. Consequently, CBZ may progress through the food chain since it has already been detected in insects [7] and in plant tissue [8]. Almeida et al. [9] detected environmentally relevant concentrations up to 9 μg/L of CBZ in the edible clams. Several tertiary processes have been used for the elimination of trace pharmaceuticals from water systems. Chemical processes, such as advanced oxidation (AOP) [10] can degrade pharmaceutically active molecules, including complete mineralization of pollutants in some cases [11]. However, these processes can also be associated with higher operational costs and complexity, depending on the specific context of their application [10]. Physical processes, such as adsorption by activated carbon (AC), are otherwise efficient and economical and they are widely applied in the treatment of contaminated water [12,13]. The reduction of pharmaceutical residuals in aqueous systems via the use of various adsorbents, including carbonaceous material [14], clays [15], silica [16], polymeric sorbents [17], and AC [18] has been the subject of extensive research interest. Multiple researchers worked on developing ways to utilize organic waste to produce the AC required for the removal of several types of contaminants. Nevertheless, it is important to acknowledge that adsorption does not degrade the pollutant but rather concentrates it into a new phase, which requires subsequent handling or disposal. Each treatment method has its own set of advantages and limitations, and the choice of method should be based on the specific requirements of the treatment scenario. Liang et al. [19] used organic matter from cauliflower roots and copper oxides to generate and activate AC. Ahmed [20] described the preparation of AC using palm stones for wastewater treatment purposes and compared the resulting yield when using different activators. Naghdi et al. [21] derived nano biochar from pine-wood residue, Vinayagam et al. [22] compared the effectiveness of multiple eco-friendly adsorbents and compared their effectiveness on multiple pharmaceuticals. The adsorption of CBZ from aqueous solutions onto AC produced from various precursors that are not biowaste has been addressed by several workers. Nielsen et al. [23] carbonized sewage sludge and fish waste to create AC to generate a low-cost alternative for CBZ removal by adsorption. Li et al. [24] investigated the removal of CBZ in synthetic wastewater using powder-activated carbon (PAC) and they reported a high removal rate. Ek et al. [25] used granular activated carbon (GAC) on treated wastewater effluent [26]. Yu et al. [27] measured the adsorption of CBZ onto two common ACs produced from coal and coconut shells; the results indicated that both types of AC could remove a substantial amount of CBZ. A number of workers have investigated the adsorption of CBZ onto other types of adsorbents. Shan et al. [28] and Fallou et al. [29] reported good removal percentages of CBZ using carbon nanotubes (CNTs) and AC fiber cloths respectively. Bui and Choi [26] and Suriyanon et al. [30] investigated the removal of CBZ using mesoporous silica-based materials while Dai et al. [31] adopted molecularly imprinted polymers (MIP). Baghdadi et al. [32] used magnetite nanoparticles and nitric acid-treated AC while Domínguez-Vargas et al. [33] used macro-porous polymeric adsorbents. Marjan Alaghmand [34] utilized humic acid, Humasorb and Montmorillonite to remove CBZ by adsorption and obtained maximum removal percentages ranging between 83.5 % and 90.5 % in deionized water and between 78.2 % and 87.0 % in wastewater. Décima et al. [18] compared different physiochemical properties and operational conditions on the sorption capacity of both AC and biochar focusing on the adsorption capacity of CBZ. It was determined that an increase in surface area and pore volume is directly linked to an increase in CBZ adsorption. Adeyanju et al. [35] explored the different types of CBZ-AC interactions where they concluded that the major mechanisms were π-π interaction, electrostatic interactions, and hydrogen bonding. They also concluded that CBZ exhibits favorable competition with other impurities because of its hydrophobic behavior and its molecular size. On the other hand, Mondal et al. [36] enhanced the adsorption of naproxen by transforming AC into a blended composite of nano-sized materials. Aldeguer Esquerdo et al. [37] investigated the removal of CBZ and diclofenac in a hybrid process using adsorption followed by oxidation, using ozonation.

From the previous discussion, it is evident that adsorption using various materials is an efficacious process for the elimination of CBZ from aqueous solutions; however, the adsorption capacities show significant variation amongst the different adsorbent types as shown in the supplementary materials Table S1. It is important to mention that most of the laboratory-scale studies were performed with high concentrations of CBZ in the aqueous phase (at the mg/L scale) whilst pharmaceuticals are encountered in the environment at trace concentrations (in the μg-ng/L range).

The efficiency of activated carbon adsorption is dependent on several important factors, such as pH, temperature, initial adsorbate concentration, contact time, and adsorbent dosage. pH affects both the ionization of the adsorbate and the surface charge of the adsorbent [38]. Temperature influences adsorption kinetics and thermodynamics. Initial concentration drives mass transfer, while contact time determines the equilibrium capacity [39]. Adsorbent dosage impacts the available surface area and overall adsorption capacity [40].

The objectives of this work are to explore the removal of a persistent pharmaceutical on activated carbon material produced from biomass waste material, date pits were used to produce an inexpensive and sustainable adsorbent material. and to determine whether the spent activated carbon can be regenerated. While the use of date pits as a precursor for activated carbon has been previously reported, this study differentiates itself by providing a comprehensive kinetic and thermodynamic analysis of CBZ uptake on date pit-derived activated carbon (DPAC). Moreover, the analysis carried out at both higher concentrations (mg/L range) and trace ambient concentrations (μg/L range) opens a greater variety of applications in real-world scenarios. The effects of physical parameters such as pH, temperature, and high versus low CBZ concentrations were also investigated. Dynamic adsorption behavior was also investigated by conducting column breakthrough analysis. The use of biomass waste to produce an inexpensive and sustainable adsorbent waste management challenges but also upholds the circular economy's principles. This alternative is less expensive and more useful at eliminating pharmaceuticals from water treatment than typical activated carbons.

2. Materials and methods

2.1. Materials

CBZ standards were purchased from Sigma-Aldrich, with a purity of ≥98 %, HPLC grade solvents including methanol, acetone, and ethanol were supplied by Sigma-Aldrich (Milwaukee, WI). Waters Oasis hydrophilic-lipophilic (HLB) cartridges (10 mg/1 cc and 200 mg/6 cc) were purchased from Supelco S.A.L. AC was prepared from date pits and olive stones obtained from a local farm in Lebanon. PAC was purchased from Supelco S.A.L. PTFE tubing, SPE supplies, and inert PTFE syringes used in these experiments were purchased from Ibrahaddad, Lebanon. Phosphoric acid (85 %) and hydrochloric acid (10 %) were also obtained from Sigma-Aldrich/Ibrahaddad, Lebanon. Nitrogen gas with a purity of >99.99 % was supplied by Chehab Gas, Lebanon. The key physicochemical characteristics of CBZ are presented in Table S2 in the Supplementary Material.

2.2. Preparation of adsorbent by H_3PO_4 activation and characterization

The activated carbon was prepared from date pits, a readily available and cost-effective biomass waste product. Date pits were chosen due to their high carbon content and low ash content, making them an excellent precursor for producing high-quality activated carbon. Additionally, utilizing date pits contributes to waste valorization and environmental sustainability. H_3PO_4 was used for activation due to its ability to produce activated carbon with a high surface area and well-developed pore structure. Compared to other activating agents like KOH, phosphoric acid is less corrosive, easier to handle, and generates fewer environmental hazards during the activation process. Furthermore, phosphoric acid activation tends to retain more oxygen-containing functional groups on the carbon surface, which can enhance adsorption capacity for polar contaminants.

Using H_3PO_4 to activate the generated carbon comes with a disadvantage in that phosphate ions might be adsorbed by activated carbon. The adsorption of phosphate ions by the generated AC can be reduced or avoided by making the sample undergo a thorough wash with distilled water. This will ensure the removal of residual and soluble phosphate compounds. In this study, the procedure to generate the AC from a carbon precursor is as follows. Firstly, the date pits were washed and then dried for 24 h at 60 °C to eliminate residual water. Secondly, the carbon precursor was mixed with a phosphoric acid solution (85 %) at an impregnation ratio of 3:1. The sample was mixed continuously for a day to allow maximal contact between the acid and the carbon before being allowed to dry overnight at 120 °C. The reason for using H_3PO_4 is that this acid is very effective in enhancing porosity and functional group formation in hydro-chars developed from cellulosic materials [41]. The activation process was carried out at 550 °C with a nitrogen flow of 150 cm^3/min thus increasing the total surface area and the pore size of the AC. Thirdly, the mix was rinsed with a 10 % solution of HCl commonly used in activated carbon production due to its efficiency in removing residual activating agents and impurities. The effectiveness of HCl in this context has been documented in previous studies, which demonstrate its ability to produce high-purity activated carbon with minimal residual contaminants [42,43]. Furthermore, Yang et al. [44] found that pretreatment with diluted hydrochloric acid significantly increased the specific surface area and pore volume of AC, leading to enhanced adsorption capacity when compared to washing with alkali solutions such as NaOH. This supports the choice of HCl in our study for improving the quality of activated carbon to ensure the removal of leftover impurities. Fourthly, the resulting AC was washed with distilled water twice, at 60 °C and room temperature, respectively. This would rid the AC of any impurity that was left from the previous stages. Fifthly, the AC was dried at 110 °C for 24 h. The standard procedure followed, ensured high-quality activated carbon was produced. The same procedure was followed to generate activated carbon from olive stones (OSAC) for comparison to DPAC. A commercial PAC was also utilized for comparative analysis.

A high-speed surface area analyzer was used to measure the AC's capacity for nitrogen adsorption/desorption (Nova 2200e; Quantachrome instruments). Before N_2 adsorption, the DPAC sample was subjected to continuous degassing for a period of 2 h at a temperature of 200 °C. To determine specific area, pore sizes, and pore volumes of the DPAC, Brunauer-Emmett-Teller (BET) theory and Non-local density functional theory (NL-DFT) method which was reported to be superior to Barrett-Joyner-Halenda (BJH) method for characterizing micropores were used, sample were analyzed using Micrometrics Gemini VII with MicroActive software version 6 [45,46]. Fourier Transform Infrared Spectrometry (Thermo Nicolet 4700) was used to characterize the adsorbents. A scanning electron microscope (SEM) operated at a voltage of 30 kV was employed to examine the AC before and after the adsorption of CBZ (Tescan). To gain further knowledge regarding the surface chemistry of DPAC, it is advisable to experimentally determine (pH_{pzc}), which is the pH value at which the surface of the material has a zero net charge (neutral charge). Below this pH, the surface is positively charged, while above this pH, the surface is negatively charged. This parameter is critical in adsorption studies as it influences the electrostatic interactions between the adsorbent and the adsorbate. For instance, when the solution pH is below the pHpzc, the positively charged surface of DPAC will favor the adsorption of negatively charged species, while at pH levels above the pHpzc, the negatively charged surface will attract positively charged species.

2.3. Sample preparation

Standard stock solutions were prepared using HPLC grade ethanol then transferred to amber shaded glass bottles, all standards were stored in a dark environment at −20 °C to avoid or reduce the chance of degradation. Working solutions were prepared by further diluting the stock solutions with ethanol resulting in ten nominal calibration standards in the range of 0.2–5 mg/L; 0.2 mg/L was the lowest detection limit (LDL). Sodium Azide (NaN_3) added to the working solutions to ensure the inhibition of any biological activity. The sample solutions for adsorption tests were prepared by adding the stock solution to ultrapure water to achieve the target

concentration. All the CBZ adsorption experiments were conducted in autoclavable bottles that were positioned in a Thermo-fisher shaker/incubator, MaxQ 6000 equipped with ambient temperature control and operated at 120 rpm. An initial amount of adsorbent was added to the test solution, at a set pH and temperature, after reaching equilibrium, samples were taken out and filtered using 1.2 mm glass microfiber filters.

2.4. Analytical technique

Solid Phase Extraction (SPE) was used for sample preconcentration and elution with 50 % ethanol, using Waters Oasis HLB cartridges. High-Performance Liquid Chromatography (HPLC-DAD) was performed with an Agilent 1260 Infinity system equipped with a quaternary pump (G1311C) and DAD detector (G1315D), utilizing an Agilent SB-C18 column (2.1 × 50 mm, 1.8 μm) [47–49].

For low concentration measurements, Agilent 6460 Liquid Chromatography-Mass Spectrometry (LC-MS/MS) was employed, following EPA Method 1694. Before use, HLB cartridges were conditioned and prepared for loading as per manufacturer's recommendations. After loading the solution, cleanup steps were employed followed by elution with 10 mL of methanol. The resulting filtrate was dried using a gentle nitrogen stream at 40 °C and reconstituted in a solution of 50 % ethanol. It is important to note that throughout the SPE procedure, PTFE syringe filters and inert syringes were used to avoid the uptake of CBZ. The EPA analytical method 1694 was validated and the statistical data analysis and the response calibration curve are presented in Table S3 and Fig. S1 respectively.

2.5. Adsorption isotherms, kinetics, and thermodynamics of CBZ solution

Understanding the adsorption kinetics is crucial for elucidating the adsorption mechanism and optimizing the design of adsorption systems. Kinetic studies provide insights into the rate of adsorption and the time required to reach equilibrium. By analyzing kinetic data, the most suitable models that describe the adsorption process, such as the pseudo-first-order or pseudo-second-order models, can be established. This information is essential for designing efficient and effective water treatment systems. Numerous studies have explored the kinetics of pharmaceutical adsorption, and this study aims to contribute to this body of knowledge by providing a comprehensive analysis of CBZ adsorption using DPAC. The experiments were conducted at two different ranges of CBZ concentrations. The first part of the experiment investigates the concentrations of CBZ in the range of 50–200 μg/L, which is normally noted in surface water and waterways contaminated with residual pharmaceuticals resulting from poorly treated or untreated wastewater. This part of the study is crucial for situations where only conventional water treatment methods are used since such practices were deemed inefficient in removing pharmaceutical residues from the effluent water [50,51]. The work was carried out using two adsorbents, the generated DPAC and commercially purchased PAC. Under these conditions, the batch was run with 10 mg of adsorbent, and the test solution was added before placing the mixture into a temperature-controlled shaker. Kinetics were evaluated at 25 °C for a duration of 24 h. Under the lower range of CBZ, several experimental runs were conducted to determine the effects of varying process conditions on the adsorption of CBZ. Temperature (25, 35, and 45 °C.), adsorbent dosage, and CBZ concentration were varied independently. The effect of the solution pH, in the range of 2–11, was also investigated. A portable pH meter (Sension + MM156 Portable Multi Meter) was utilized for the measurements. Additional experiments compared olive stone activated carbon (OSAC) and PAC for lower CBZ concentrations. OSAC was produced following the same procedure as DPAC to ensure consistency.

The second part of the study aimed at replicating typical CBZ concentrations found in wastewater effluents ranging from 2 to 10 mg/L [52]. The higher concentration batch runs were particularly useful in assessing the need for phenomenological modeling to overcome the shortcomings of pseudo first and second-order experiments to model CBZ removal with DPAC. To that end, a series of additional experiments were designed to assess the impact of fluctuating CBZ (2, 5, 8, and 10 mg/L) concentrations and pH levels (3, 7, and 10). Utilizing a traditional bottle-point approach, multiple sets of batch experiments were conducted over 24 h. Each set involved adding 25 mg of DPAC to 0.1 L of distilled water, which was then spiked with CBZ. In total, 9 experiments were carried out to fulfill this purpose, and throughout these experiments, samples were continuously agitated at 120 rpm and maintained at a constant temperature of 25 °C. The samples were collected at predetermined time intervals and sacrificed for analysis. Controls without DPAC were run concurrently with each experiment to establish a baseline.

The influence of temperature on CBZ adsorption was also examined to determine thermodynamic parameters such as changes in Gibbs free energy (ΔG), enthalpy (ΔH), and entropy (ΔS). The amount of CBZ adsorbed at equilibrium (q_e) was determined using:

$$q_e = \frac{(C_0 - C_e)V}{m} \tag{1}$$

where q_e is in mg/g, C_o is the initial CBZ concentration in mg/L, C_e is the equilibrium CBZ concentration in mg/L, V is the total solution volume in L and m is the mass of adsorbate in g. The models (Table S4) Langmuir, Freundlich, Dubnin-Radushkevich, Toth and Sips were selected to fit the sorption isotherms [53]. Statistical analysis and mathematical modeling were carried out using RStudio [54] and Microsoft VS code. Each experiment was conducted in triplicate to ensure the robustness and reliability of the results.

2.6. Regeneration experiments

The regeneration of the spent AC using methanol as the regeneration solvent was investigated. 0.5 g of spent adsorbent was separated from the solution and placed in a clean beaker containing a measured volume (50 mL) of solvent. The solvent-exhausted

carbon mixture was shaken for 4 h and the regenerated DPAC was rinsed and washed with distilled water. The wet DPAC was dried at 80 °C. Adsorption experiments were conducted on the regenerated DPAC using the procedure described in section 2.3 and the experiment was stopped when equilibrium was reached. The adsorption/regeneration experiments were repeated for four cycles. The adsorption capacity applicable for one cycle was determined from:

$$q_{e,i} = \frac{(C_{0,i} - C_{e,i})}{m} V_i \tag{2}$$

where the subscript i represents the cycle number. The regeneration efficiency, RE, is required to determine the effectiveness of the regeneration method:

$$RE = \frac{q_r}{q_e} \times 100\ \% \tag{3}$$

where q_e is the adsorption capacity of fresh DPAC in mg/g, q_r is the adsorption capacity of the regenerated DPAC after completion of all the adsorption-desorption experiments, in mg/g.

2.7. Fixed bed adsorption study

Understanding the behavior of CBZ adsorption onto the generated adsorbent in a fixed bed continuous mode is required to determine design parameters for CBZ removal and to evaluate and optimize the systems performance. This is done so by running a column breakthrough analysis. This approach is also intended to establish the mathematical models that may be used to provide accurate predictions of the CBZ-adsorbent interactions for larger scale operations. CBZ was introduced into the column at a rate of 5 mL/min and concentrations of 2, 4, and 10 mg/L. Moreover, to determine the effects of the flow rate, one CBZ concentration was maintained while the rest were subjected to varying flows. Additionally, the experiments were conducted with three iterations for higher redundancy. To ensure the reliability and robustness of the results, each experiment was conducted in triplicate.

Quartz columns were packed with 70 g of the DPAC produced in this work and another set of columns packed with Ottawa sand (inert material) were run as controls. All columns were mounted with identical metallic screens at both ends to ensure that the respective packing material did not escape from the column. The flow of the solution was maintained using low flow pumps (Cerampump FMI QG 50) with a maximum of 10 mL/min as well as a CSC-W stainless steel head fitted pump and PTFE tubing.

3. Results and discussion

3.1. Adsorbent characterization

The BET analysis of the derived DPAC revealed a specific surface area of 309 m^2/g, and a pore volume of 0.264 cm^3/g. The NLDFT pore size distribution analysis further substantiated the hierarchical nature of the DPAC's pore structure, with the majority of pores predominantly concentrated at 1.86 nm, 2.73 nm, and 3.43 nm as illustrated in Fig. 1a.The BET surface area of the DPAC falls within the range of data reported in the literature for date pits (78.89–770 m^2/g) [55–57]. The total pore volume obtained in this work is also comparable with earlier studies on date pits (0.17–0.66 cm^3/g) [55–57]. The nitrogen adsorption-desorption isotherms are shown in Fig. S2 where it can be noted that the adsorption volume increased rapidly up to a relative pressure ratio, P/P_0, of 0.1, which may be

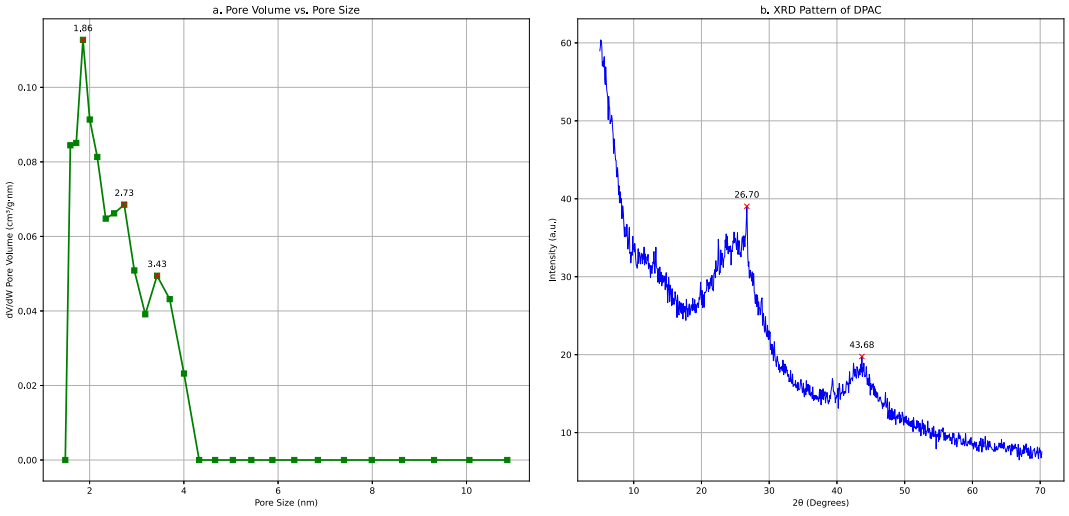

Fig. 1. (a) NL-DFT pore size distribution and (b) XRD Patterns of DPAC.

attributable to the existence of micropores [58]. Moreover, a gradual and steady increase in the adsorbed volume throughout the range of relative pressures is typical for mesoporous materials. In addition, desorption isotherm exhibited a hysteresis loop at P/P_0 above 0.4, which is a feature of a type IV isotherm and is often linked with the occurrence of pore condensation [55].

The XRD pattern of DPAC in Fig. 1b showed that the activated carbon had a structure characterized by the presence of (002) and (100) planes at $2\theta = 26.7$ °C and 43.68 °C [59,60] The presence of these peaks indicates that the activated carbon derived from date pits contains both graphitic and amorphous carbon structures.

SEM images shown in Fig. 2 reveal the surface morphology of the adsorbent precursor and AC produced by chemical activation. The examination of raw date stones shows interconnected porosity and formation of aggregates. After chemical activation, the porosity is more developed and relatively large and abundant and non-uniform in shape with elliptical pores. The images indicate that the chemical activation of date pits results in a relatively smooth surface with scattered pores of various sizes. Physical sorption of pharmaceuticals is more likely to occur on highly porous AC.

Fig. 3, which depicts the FTIR spectrum for the adsorbent precursor, indicated the presence of several different functional groups namely alkene, aromatic, alcohol, ester, ether, and hydroxyl. The sample shows IR bands at 3400- 3600 cm^{-1} which are ascribed to the -OH stretching of the hydroxyl groups [55,57]. The sample also shows peaks at 2926 and 2870 cm^{-1}, which correspond to C-H stretching in alkyl groups. The bands appearing at 1400–1600 cm^{-1} are ascribed to C=C stretching in aromatic rings, and the ones at 1000–1200 cm^{-1} are attributed to C-O stretching in ether groups. Finally, the bands appearing at 1600–1700 cm^{-1} correspond to the carbonyl group. The IR spectrum of the activated carbon exhibits the same shape, which indicates that both materials have the same functional groups. The peaks observed at 2926 and 2870 cm^{-1} in the raw precursor disappear once the material is impregnated with H_3PO_4. Also, the FTIR spectrum of DPAC shows lower transmission (thus higher adsorption) percentages at all observed bands compared to the raw precursor, suggesting a greater density of functional groups on the surface of DPAC than on raw date pits. Furthermore, the pH_{pzc} of the AC was found to be equal to 3.4 (Fig. S3).

There are several factors to consider when choosing a material for a particular application, including the kind of pollutants, cost-effectiveness, and operating circumstances. When comparing DPAC to granular activated carbon (GAC) and PAC, DPAC exhibits similar adsorption efficiencies due to its high surface area and pore volume, which are critical factors in adsorption capacity. However, there are several disadvantages to using DPAC. For example, it has been observed that in the presence of organic matter and micro-contaminants, the adsorption capacity is lower than that of GAC [61]. Reduced efficiency and competitive adsorption may result from this. However, materials such as biochar, which is made by pyrolyzing biomass, have been shown to work as well as or better in environments with a lot of pollutants due to their unique surface chemistry and pore structure [62]. Understanding the impact of different ions found in actual water matrices on DPAC's adsorption performance is essential to comprehending its wider applicability. Studies reveal that the adsorption capacity of carbamazepine and related pollutants can be considerably impacted by common anions such as Cl^-, NO_3^-, SO_4^{2-}, and cations such as Ca^{2+}, and Mg^{2+} due to competitive adsorption and surface charge variations. Viegas et al. [63] investigated the effect of these ions on the adsorption of carbamazepine onto organoclays and found that certain ions, particularly divalent cations, can hinder the adsorption efficiency by occupying active sites on the adsorbent surface or altering its charge properties. The study's findings demonstrated that while organoclays could effectively adsorb CBZ, the adsorption capacity was decreased by more than 20 % when ions like Ca^{2+} were present, highlighting the necessity of considering ion interference in real-world water applications. It is expected that DPAC would behave in a similar manner and active sites might be depleted in the presence of competing contaminants.

3.2. CBZ adsorption isotherms

Results for the lower concentration experiments and the calculated model parameters are shown in Table 1, Adsorption capacities predicted by the models (q_{cal}) were compared to the experimental values (q_{exp}) using several statistical parameters. These included the standard deviation method, the R^2 coefficient, and the Chi-square χ^2 test. These are given by the following formulae:

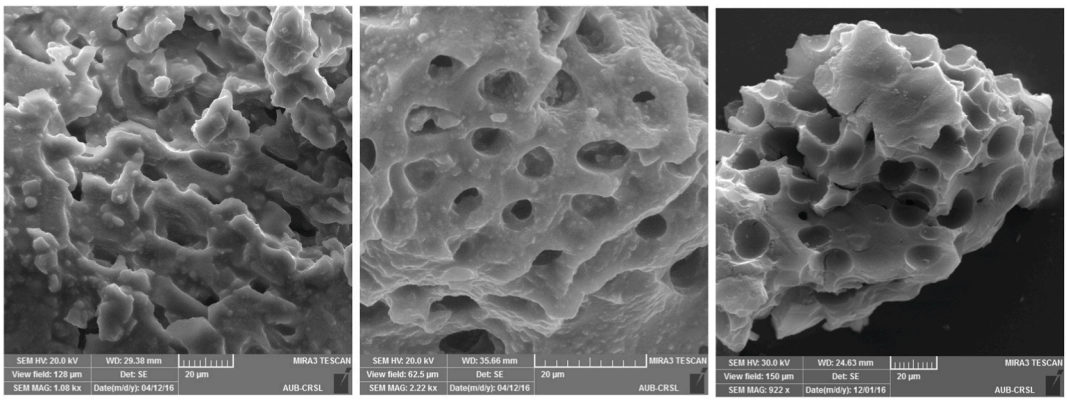

Fig. 2. SEM images of (a) raw date pits and (b) DPAC (c) DPAC washed.

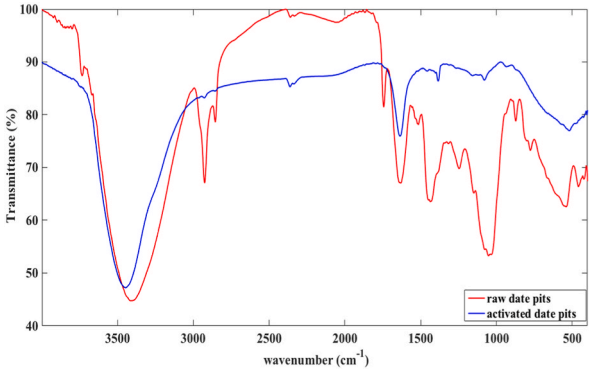

Fig. 3. FTIR of raw and activated date pits.

Table 1
Parameters of adsorption equilibria isotherms under lower concentrations of CBZ.

Model	Parameter	Adsorbent				
		DPAC[a]			OSAC[b]	PAC[c]
		25°C	35°C	45°C	25°C	25°C
Langmuir	q_m (mg/g)	7.08	7.17	7.23	7.44	14.39
	K_L (L/mg)	9.37	10.12	10.32	8.37	12.79
	R_L	0.45	0.43	0.42	0.50	0.36
	R^2	0.999	0.998	0.999	0.997	0.999
	DS	0.30	0.26	0.24	0.26	0.67
	X^2	0.03	0.04	0.03	0.02	0.08
Freundlich	*1/n*	0.73	0.73	0.72	0.76	0.69
	K_f (mg/g)(1/mg)^n	19.58	20.30	20.38	20.60	42.10
	R	0.997	0.995	0.997	0.994	0.992
	DS	0.22	0.21	0.22	0.22	0.26
	X^2	0.07	0.06	0.07	0.07	0.24
Sips	q_m (mg/g)	6.83	6.64	7.01	5.65	11.74
	K_s (L/mg)$^{1/s}$	10.52	12.85	11.32	20.60	28.54
	S	0.99	0.96	0.99	0.87	0.87
	R^2	0.964	0.956	0.960	0.928	0.910
	DS	1.08	1.28	1.57	2.10	3.26
	X^2	0.56	0.79	0.61	0.81	3.81
Toth	q_m (mg/g)	6.75	6.64	6.63	4.69	10.30
	K_t (L/mg)$^{1/t}$	10.88	14.26	13.49	58.88	72.05
	T	1.04	1.11	1.09	1.66	1.57
	R^2	0.966	0.963	0.963	0.955	0.910
	DS	0.98	0.92	1.13	0.80	1.26
	X^2	0.51	0.51	0.55	0.31	1.58
Dubnin Radushkevich	q_m (mg/g)	6.47	6.67	6.79	6.50	14.37
	β 10^{-8} (mol^2/J^2)	1.80	1.55	1.65	1.88	1.64
	E (kJ/mol)	5.26	5.67	5.50	5.16	5.51
	R^2	0.999	0.998	0.999	0.999	0.998
	DS	1.00	0.99	1.00	1.01	1.00
	X^2	0.19	0.15	0.48	0.20	0.33

[a] DPAC: Date pit AC.
[b] OSAC: Olive stone AC.
[c] PAC: Powdered AC.

$$DS = \sqrt{\frac{\sum \left[\left(q_{e\ exp} - q_{e\ cal} \right) / q_{e\ exp} \right]^2}{N - 1}} \tag{4}$$

$$R^2 = 1 - \frac{\sum \left(q_{e\ exp} - q_{e\ cal} \right)^2}{\sum \left(q_{e\ exp} - q_{e\ avg} \right)^2} \tag{5}$$

$$\chi^2 = \sum_{i=1}^{n} \left[\frac{\left(q_{e\ exp} - q_{\ e\ cal} \right)^2}{q_{e\ cal}} \right]_i \tag{6}$$

where *n and N* in equations (3) and (5) represent the number of experimental points, *DS* and χ^2 should be as small as possible, while R^2 should be as close to one as possible. When more than one model is statistically acceptable, the Chi-square χ^2 test was used, and the lowest χ^2 value corresponds to the best-fit model. The experimental and fitted data are shown in Fig. 4 for the five models. A comparison of the adsorption models shows that experimental data show a high correlation with two isotherm models, namely the Langmuir and Freundlich models.

From the data in Table 1, q_m, the maximum monolayer coverage capacity estimated from the Langmuir isotherm, was determined to be 7.08, 7.17, and 7.23 mg/g at 25, 35, and 45 °C respectively. From the data calculated, R_L, the separation factor, is greater than 0 but less than 1 indicating that adsorption on DPAC is favorable. Other studies investigating the removal of CBZ onto carbonaceous adsorbents have also reported that the adsorption was best fitted to the Langmuir isotherm [33,64]. The Freundlich model also appears

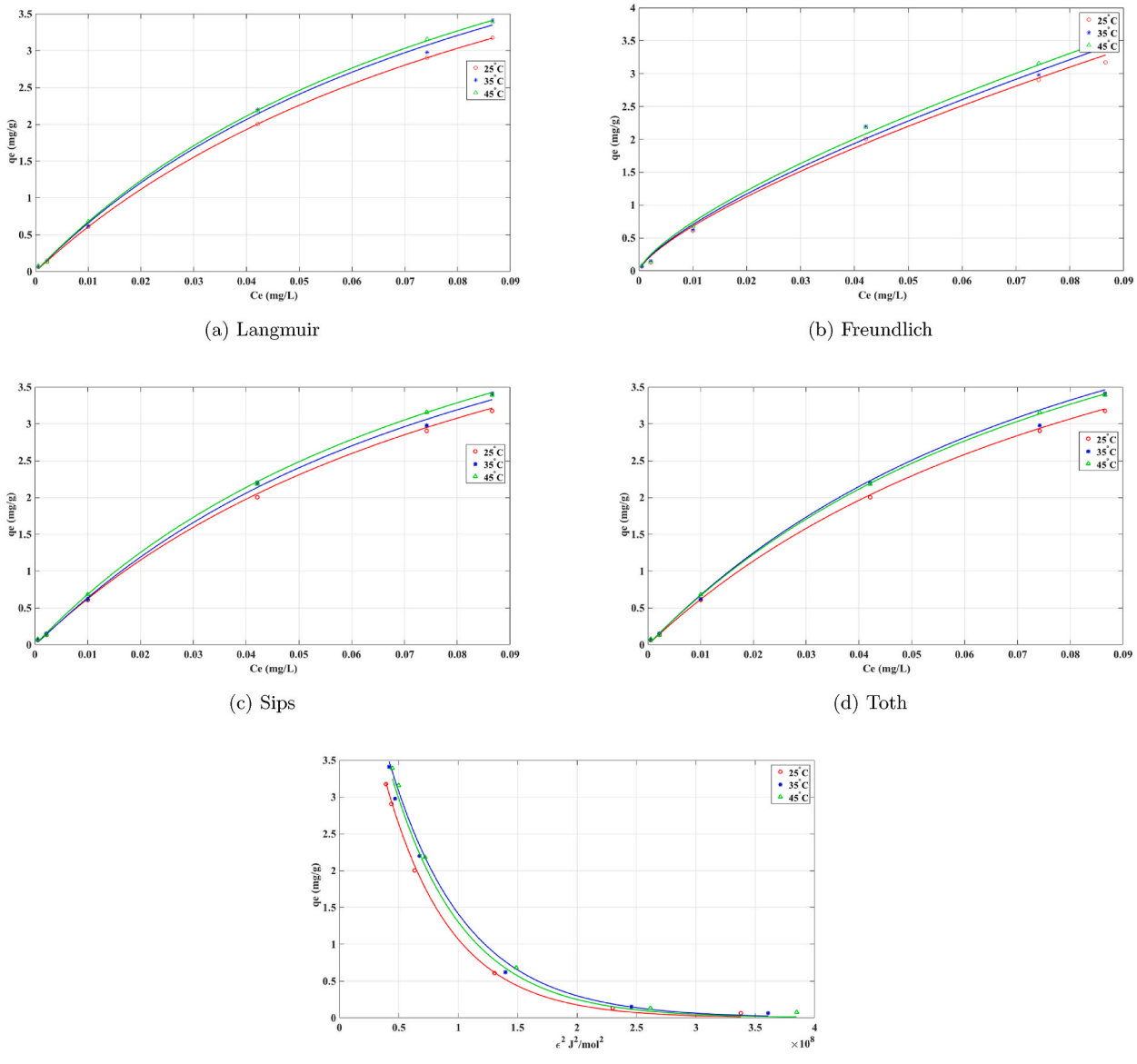

Fig. 4. Equilibrium adsorption isotherm for DPAC by (a) Langmuir model, (b) Freundlich model, (c) Sips model, (d) Toth model, (e) Dubinin-Radushkevich model.

to be a good fit for the experimental data of adsorption of CBZ onto DPAC as the constant *n* lies between 1 and 10 for all three temperatures (1.3652, 1.3739, and 1.3842 at 25, 35, and 45 °C respectively). The results suggest that chemisorption may take place since the resulting *1/n* value is below unity [53]. Other studies also showed the Freundlich model to be the best-fit model for the adsorption of CBZ on various other types of AC [25,26].

It is noted from Table 1 the Langmuir and Freundlich models also provide the most satisfactory representation of the equilibrium data for the OSAC and commercial PAC, which implies that similar adsorption mechanisms govern CBZ behavior in the presence of the three adsorbents. OSAC shows a slightly higher adsorptive capacity than DPAC. However, the commercial AC achieved a removal capacity of 14.4 mg/g, being significantly higher than those observed for DPAC and OSAC. This variation may be due to the significantly higher surface area of commercial carbon.

From Table 2, q_m, estimated from the Langmuir isotherm, was determined to be 14.74, 14.86, and 14.89 mg/g at 25, 35, and 45 °C respectively for DPAC at higher CBZ concentrations. It is important to note that q_m is significantly higher at ~15 mg/g for higher CBZ concentrations compared to ~7 mg/g for lower concentrations. This indicates higher adsorption capacity is achieved when more adsorbate is available.

The Langmuir model, which assumes monolayer adsorption on a homogenous surface, provided the best fit to the experimental data. When assessing the variation in the Langmuir constant K_L, representing the affinity between the adsorbate and the adsorbent, it is generally expected that K_L will increase with a higher concentration gradient due to the greater driving force for adsorption. However, in this study, the opposite effect was observed: a decrease in the K_L value at higher CBZ concentrations. This reduction may be attributed to the saturation of the higher energy adsorption sites on the DPAC surface. Once these sites are occupied, adsorption occurs on sites with lower binding affinities, leading to the observed decrease in the K_L value. This phenomenon indicates that while the initial adsorption at lower concentrations occurs at high-affinity sites, further adsorption at higher concentrations may involve less energetically favorable sites, thereby lowering the overall K_L term. These findings suggest that the adsorption process of CBZ onto DPAC is governed by a balance between the availability of high-affinity sites and the concentration of CBZ in the solution.

The separation factor R_L is between 0 and 1 indicating favorable adsorption, similar to the lower concentration results. The Freundlich model also appears to fit the experimental data well, with 1/n values below 1 suggesting that a similar mechanism to that of lower CBZ concentrations may be taking place, however, K_f is higher and 1/n lower at higher concentrations, indicating more favorable adsorption which aligns with the higher adsorption expected. Both the Toth and Dubinin-Radushkevich models gave high R^2 values (>0.95) across the temperatures, indicating it may also accurately describe the adsorption behavior. The q_m values from the Toth model were slightly higher than the Langmuir model. The model also fits the data reasonably well based on the high R^2 values. Sips, Toth, and Dubinin-Radushkevich models show similar trends of higher qm values at higher CBZ levels due to greater adsorption.

Table 2
Parameters of adsorption equilibria isotherms using DPAC under high CBZ concentration (2–10 mg/L).

Model	Parameter	DPAC high CBZ concentration		
		25°C	35°C	45°C
Langmuir	q_m (mg/g)	14.74	14.86	14.89
	K_L (L/mg)	1.98	2.12	2.29
	R_L	0.40	0.45	0.43
	R^2	0.988	0.978	0.989
	DS	0.20	0.22	0.22
	X^2	0.01	0.02	0.02
Freundlich	*1/n*	1.22	1.35	1.28
	K_f (mg/g)(1/mg)^n	9.14	11.62	10.42
	R^2	0.999	0.999	0.999
	DS	0.20	0.24	0.20
	X^2	0.04	0.03	0.03
Sips	q_m (mg/g)	15.06	14.96	14.83
	K_s (L/mg)$^{1/s}$	1.98	2.12	2.29
	S	0.89	0.84	0.91
	R^2	0.957	0.960	0.970
	DS	0.80	0.77	0.62
	X^2	0.45	0.72	0.77
Toth	q_m (mg/g)	16.01	15.67	15.50
	K_t (L/mg)$^{1/t}$	2.75	2.33	2.12
	T	0.91	0.88	0.93
	R^2	0.961	0.968	0.979
	DS	0.61	0.62	0.82
	X^2	0.28	0.21	0.22
Dubnin Radushkevich	q_m (mg/g)	13.45	13.58	13.64
	$\beta\ 10^{-8}$ (mol^2/J^2)	0.024	0.020	0.018
	R^2	0.956	0.959	0.969
	DS	1.11	1.12	1.33
	X^2	0.24	0.25	0.25

K_s, K_t, and E values vary inconsistently between concentrations across models, indicating a complex impact on bonding affinity.

In summary, Langmuir, Freundlich, Sips, Toth, and Dubinin-Radushkevich models were used to characterize the adsorption of CBZ on DPAC. While the Langmuir model assumes homogeneous adsorption sites with uniform adsorption energies, the Sips and Toth models are particularly suited to systems where adsorption sites exhibit varying affinities, thereby capturing the heterogeneity of the adsorbent surface. The application of these models, which all showed good fits to the experimental data, allows for an omprehensive understanding of the adsorption mechanism, indicating that the adsorption of CBZ on DPAC involves both homogeneous and heterogeneous sites with varying affinities and potential mechanisms.

3.3. Phenomenological modeling using LDF

Fig. 5 depicts the change of CBZ with time while Table 3 summarizes the parameters for pseudo-first order and the pseudo-second-order kinetic rates, the model parameters fit the lower concentration experimental data quite well (R^2>0.9). The pseudo-first-order rate model assumes that physisorption is dominant where adsorption occurs through weak interactions such as van der Waals forces. On the other hand, the pseudo-second-order rate equation is often linked to chemisorption, which involves stronger chemical interactions between the adsorbate and the adsorbent surface. Given the results of our kinetic modeling and the supporting FTIR analysis, it can be inferred that both physisorption and chemisorption mechanisms are involved in the adsorption of CBZ onto DPAC. This dual mechanism is consistent with the observations discussed in section 3.2, where the minimal changes in FTIR spectra suggest that while chemisorption occurs, it may not be the dominant mechanism, and physisorption plays a significant role in the adsorption process. It is important to mention that physisorption normally occurs where the CBZ pore size is approximately equal to 10 Å, which is below the average pore size of DPAC (31 Å), justifying the assumption that CBZ molecules will be able to penetrate the interior surfaces of the adsorbent.

As opposed to the accurate fit observed at lower concentrations of CBZ, the pseudo-first and second-order models were inadequate in representing the adsorption data at higher concentrations. This discrepancy indicates that these models demonstrate theoretically inconsistent trends with experimental data, a finding that has been corroborated in multiple studies [65–67]. [65–67]. The observed inconsistencies led to the adoption of the Linear Driving Force (LDF) model. LDF is a widely recognized approach in adsorption kinetics, offering a more mechanistic insight into the adsorption process [68], and unlike empirical models, is grounded in the principle of mass transfer [69]. Due to its flexibility, the model is particularly effective in describing the rate of adsorption, accounting for the resistance to mass transfer [70], especially in scenarios involving higher solute concentrations [71].

The fundamental equation of the LDF model is expressed as:

$$\frac{d\,q_t}{d\,t} = k_L\,(q_e - q_t\,) \tag{7}$$

where q_t is the amount of adsorbate on the adsorbent at time t, q_e is the equilibrium concentration of the adsorbate on the adsorbent, k_L is the LDF rate constant. Across a range of pH levels and starting CBZ concentrations, the derived model parameters, which are displayed in Table 4, show an overall high degree of correlation between the LDF model predictions and the experimental data. R^2 values varied between 0.92 and 0.98 indicating a strong correlation between the model predictions and the experimental outcomes. This observation further establishes the reliability of the LDF model in capturing the kinetics of CBZ adsorption and indicates the likelihood that sorption process is more efficient and predictable in a neutral pH environment. The kinetic data presented in Fig. 6 show the fitted

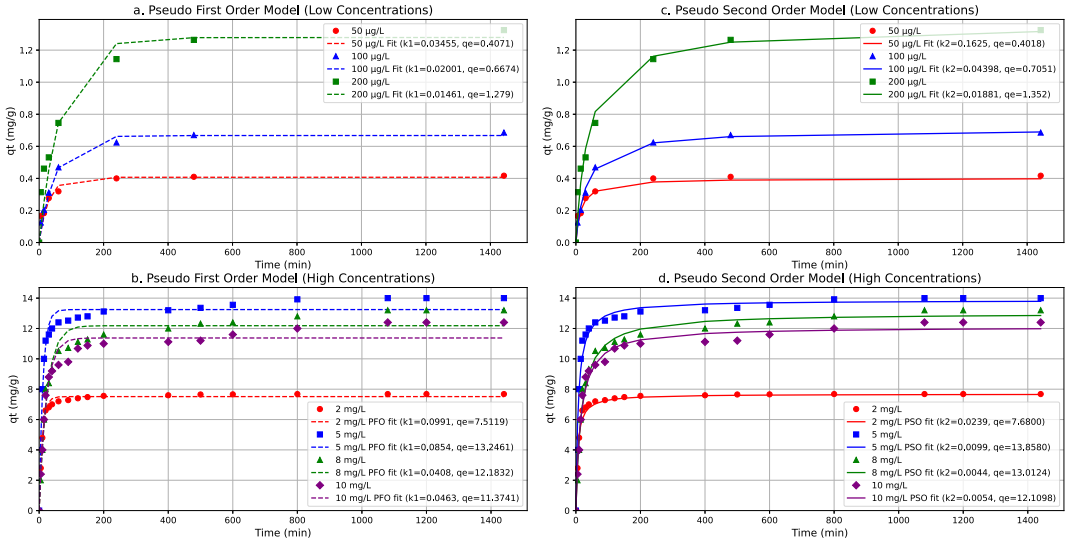

Fig. 5. Adsorption kinetics of CBZ concentrations by pseudo-first-order and pseudo-second-order models.

Table 3
Pseudo-first order model and pseudo-second-order model constants and correlation coefficients for adsorption of CBZ onto DPAC at 25 °C.

C_0 mg/L	q_e exp (mg/g)	Pseudo first order			Pseudo second order		
		R^2	K_1 (min^{-1})	q_e cal (mg/g)	R^2	K_2 ($g.mg^{-1}.min^{-1}$)	Q_e cal (mg/g)
0.05	0.41	0.940	0.0346	0.41	0.960	0.1625	0.42
0.1	0.69	0.980	0.0200	0.67	0.999	0.04398	0.71
0.2	1.34	0.940	0.0146	1.28	0.972	0.01881	1.35
2	7.68	0.991	0.0991	7.51	0.980	0.02385	7.68
5	14	0.977	0.0854	13.25	0.978	0.00988	13.86
8	13.2	0.967	0.0408	12.18	0.986	0.00438	13.01
10	12.4	0.963	0.04635	11.37	0.983	0.00542	12.11

Table 4
Derived model parameters for each experiment.

Experiment	pH	Initial CBZ concentration	R^2	RSS	K_L
Experiment 1	7	2	0.9863	1.0	0.093688
Experiment 2	7	5	0.9533	18.6	0.069125
Experiment 3	7	8	0.9644	34.2	0.017188
Experiment 4	7	10	0.9854	17.7	0.027141
Experiment 5	3	2	0.9737	1.8	0.124438
Experiment 6	3	4	0.9307	31.9	0.047438
Experiment 7	3	8	0.9906	11.8	0.016797
Experiment 8	10	2	0.9627	3.02	0.021625
Experiment 9	10	5	0.9273	10.7	0.013625

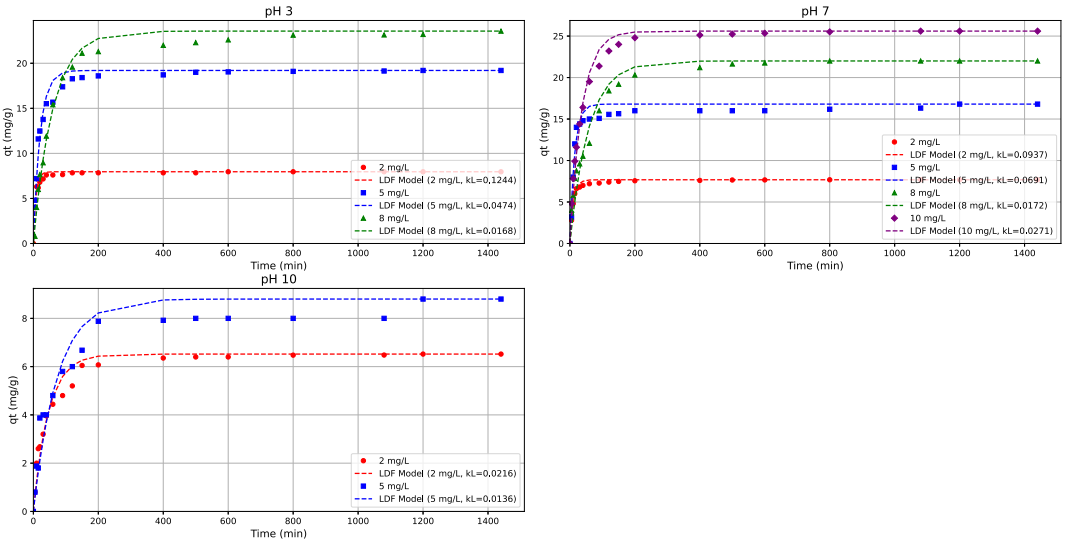

Fig. 6. LDF model fittings for high concentrations of CBZ.

LDF model (red curve) aligning closely with the experimental points (blue dots) for CBZ adsorption onto DPAC. A somewhat contradictory observation could be interpreted from experiment 5 (pH = 3, C_i = 2 mg/L) resulting in the highest k_L suggesting that acidic conditions may enhance the adsorption rate for lower contaminant levels. When comparing initial CBZ concentrations, the model suggests that lower concentrations tend to have higher k_L values, indicative of a more rapid approach to equilibrium. The optimal conditions appear to be at a neutral pH with the lower initial CBZ concentrations as reported with the R^2 and residual sum of squares (RSS) values. However, the utility of the LDF model across varying pH levels and higher concentrations also suggests its adaptability under various treatment scenarios.

3.4. Adsorption thermodynamics

The changes in the enthalpy and entropy are determined from a plot of $ln\ K_D$ vs. $1/T$ as shown in Fig. S5. The lower concentration experimental results reveal that ΔH° was endothermic and equal to 31.55 kJ/mol while ΔS° was equal to 0.1393 kJ/mol/°K. On the

other hand, ΔG° was equal to −9.96, −11.36, and −12.75 kJ/mol at 25, 35, and 45 °C respectively. This increase in negative magnitude with the increase in temperature can signify the spontaneity of the adsorption of CBZ onto DPAC. Table 5 shows the results under the higher CBZ concentration range.

Because of the weak connections between the carbon adsorbent and adsorbate, heat is needed to enhance adsorption, as evidenced by the positive enthalpy change (ΔH), which suggests an endothermic reaction. Concurrently, it is postulated that the release of hydration water and the unhindered mobility of the adsorbate molecules following adsorption were responsible for the positive entropy change (ΔS) which indicates a greater randomness at the solid-solution interface. The adsorption process' intrinsic spontaneity was confirmed by the fact that the Gibbs free energy change (ΔG) was negative under all examined settings. ΔG became increasingly negative as the temperature rose from 25 °C to 45 °C, which was in line with the endothermic behavior. It is not clear from the table alone how ΔG will fluctuate with the increase in the initial concentration (C_i). The thermodynamic viability of the process is determined by several criteria, including the availability of adsorbent sites, the strength of the interaction, and the total adsorption capacity, as demonstrated by the trends in ΔH, ΔS, and ΔG with varying initial adsorbate concentration.

It has been previously reported that for physisorption, ΔG° falls in the range of −20 to 0 kJ/mol while for chemisorption it is between −80 and −800 kJ/mol [72]. Hence, for the values of ΔG° obtained in this study, the adsorption of CBZ onto DPAC falls within the physisorption range. The change in ΔG° with the temperature change may be a result of the adsorbate molecules becoming more mobile in the solution leading to a higher affinity of adsorbate on the adsorbent at the higher temperatures [73]. It has been postulated that during physical adsorption ΔH° falls in the range of 2.1–20.9 kJ/mol, while for chemical adsorption ΔH° falls in the range of 80–200 kJ/mol [73]. Given the magnitude of ΔH° calculated in this work, the adsorption of CBZ by the DPAC can be attributed to physio-chemical processes. A positive value of ΔS° reflects the affinity of CBZ towards the adsorbent and corresponds to increased randomness at the solid/liquid interface.

3.5. Effect of operating conditions

3.5.1. Effect of temperature

The activation energy E_a for the adsorption of CBZ onto DPAC was determined using the Arrhenius equation:

$$k = A_R e^{-E_a/RT} \tag{8}$$

where:

k is the rate constant of the reaction performed at 25, 35 and 45 °C.

A_R is the Arrhenius pre-exponential factor or frequency factor.

E_a is the activation energy.

R is the gas constant (8.314 J/(mol·K)).

T is the temperature in Kelvin.

For this purpose, lnk was plotted vs $\frac{1}{T}$ and the activation energy was determined from the slope and found to be equal to 25.73 kJ/mol as can be seen in Fig. S6. It has been postulated that E_a for physical adsorption varies between 5 and 40 kJ/mol, whereas for chemical adsorption, E_a is reported to be in the range of 40–800 kJ/mol since chemical adsorption is more specific than physical adsorption and involves stronger forces [73]. In this study, the value for E_a indicates that the adsorption of CBZ onto DPAC is of the physisorption type.

3.5.2. Effect of pH

When compared to temperature variation, the adsorption affinity of CBZ showed less significance when assessing the impact of change in solution pH, which is attributable to CBZ's high pK_a value of 13.96. Given the nature of CBZ molecules, such an observation could be related to the negligible variation in the ionic state from the neutral to the ionized form of CBZ which ensures that the adsorbate remains neutral throughout the pH range considered. Given that CBZ is composed of two benzene rings, one azepine group, and an amide group, adsorption involves hydrogen bonding between the oxygen groups present on the DPAC surface and nitrogen atoms of CBZ and/or van der Waals forces. However, as noted in section 3.3 lower pH seemed to improve the uptake kinetics, this showed the need to perform further statistical analysis to accurately determine the significance of pH variations. To that end, a two-way ANOVA test was conducted the output p-values at 95 % confidence for the effect of pH was greater than 0.05 which suggests that there are no statistically significant differences in K_L due to pH variations. Furthermore, the Tukey HSD post-hoc tests confirm these findings. It should be noted that p-values are relatively close to the cutoff, which might indicate a trend that could become significant with more data points or in a more controlled experimental setup.

Table 5
Experimental results for high CBZ concentrations.

C_i (mg/L)	ΔH (kJ/mol)	ΔS (kJ/(mol*K))	ΔG at 25 °C (kJ/mol)	ΔG at 35 °C (kJ/mol)	ΔG at 45 °C (kJ/mol)
2	82.89	0.31	−10.83	−13.97	−17.12
5	30.37	0.13	−8.03	−9.32	−10.6
8	7.68	0.04	−5.67	−6.12	−6.57
10	10.76	0.05	−4.89	−5.42	−5.94

3.6. Suggested CBZ removal mechanism

When CBZ is adsorbed from an aqueous solution onto AC, the following sequence of steps are postulated to take place: transport of CBZ in the solution; transport of CBZ from the solution to the external surface of DPAC, this is known as "boundary film diffusion"; transfer of CBZ from the external surface to the intra-particle active sites, known as "the intra-particle diffusion"; finally, the incorporation of CBZ onto the active sites [74,75]. [74,75]. When rapid mixing is employed, the first step is often omitted; this is also valid for the last step of this process i.e., the adsorption of CBZ on the internal surfaces of the AC. The underlying assumption is that organic molecules are adsorbed onto porous adsorbents at an accelerated pace and therefore the impact of this steps is negligible [75]. Therefore, in principle, the "boundary layer diffusion" step and the "intra-particle diffusion" step are the only possible rate controlling processes. The intra-particle diffusion model, suggested by Weber and Morris [75], is usually adopted to establish the potential rate-limiting step. The equation for this model is given by:

$$q_t = K_{id}\, t^{0.5} + C_b \tag{9}$$

where q_t is the quantity of adsorbed CBZ, K_{id} is the intra-particle diffusion parameter and C_b is the boundary layer thickness. If the intra-particle diffusion was the rate-controlling step, then a plot of q_t versus $t^{0.5}$ will yield a straight line passing through the origin. However, the plot for the experimental data obtained at 25 °C shows a non-linear behavior as] seen in Fig. 7. The adsorption process plot exhibits multi-linear regions, which can be divided into two portions. The first portion, with a steep slope, likely represents external diffusion by macro-pores and meso-pores [76]. The second portion, with a very low slope, represents intraparticle diffusion by micropores. This multi-stage behavior suggests that different mechanisms are involved at different stages of the adsorption process.

During the early stages of CBZ adsorption onto DPAC, external diffusion appears to be an important rate-limiting step. The change of CBZ concentration with time during this initial stage can be evaluated using the following equation:

$$\frac{dC}{dt} = -k_L A(C - C_s) \tag{10}$$

where k_L is the external mass transfer coefficient, A is the surface area (416 m^2/g) available for mass transfer, C is the CBZ bulk concentration and C_s is the CBZ surface concentration in mg/L. At $t = 0$, $C = C_0$ and the surface CBZ concentration is negligible, which implies that the intra-particle diffusion is not relevant. Consequently, the change of CBZ concentration can be expressed as:

$$\left.\frac{d\,C/C_0}{dt}\right|_{t\to 0} = -k_L A \tag{11}$$

The value of $k_L A$ is determined from the slope of a C/C_0 vs t plot. Kinetics data obtained at three initial concentrations were used to calculate the external mass transfer coefficients. As shown in Table S5, an increase in the initial concentration of CBZ resulted in a decrease in mass transfer to the surface. Accordingly, the external mass transfer resistance is significant during the first period of adsorption and, as has been noted by several previous studies, cannot be negligible even at high agitation velocities. In the second portion of the plot, it appears that diffusion of CBZ from the external surface to the intra-particle active sites is the rate-limiting step and the rate constant K is determined using the Webb-Morris model described earlier (eq. (8)). The values of K are listed in Table S5 and as can be seen they tend to increase with the increasing CBZ initial concentration; this may be attributed to a larger driving force enhancing adsorption at the higher concentrations.

CBZ adsorption onto DPAC was initially suggested to involve both physisorption and chemisorption mechanisms. To better

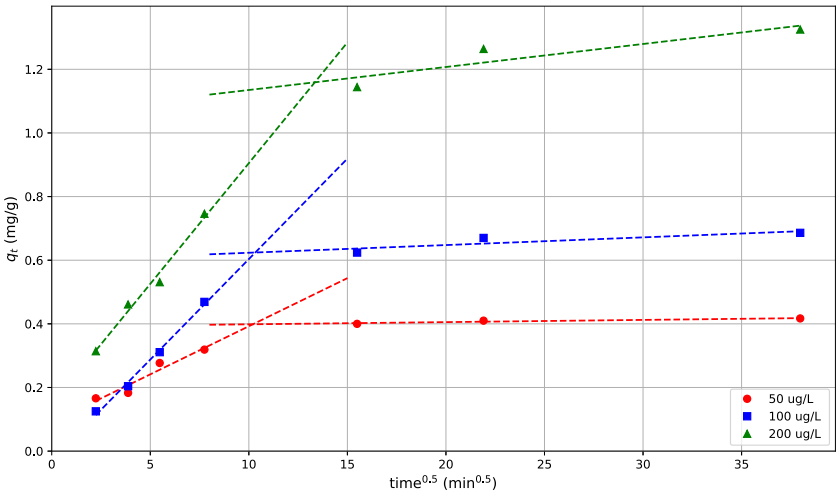

Fig. 7. Plot of q_e versus $t^{0.5}$ at 25 °C at various concentrations.

understand these interactions, FTIR spectra were analyzed for DPAC before and after CBZ adsorption, as shown in Fig. 8. FTIR spectra of DPAC before and after the adsorption of CBZ show minimal changes in the characteristic absorption bands, indicating that most of the adsorption process involves weak physical interactions. These could include van der Waals forces and hydrogen bonding, which do not significantly alter the functional groups on the DPAC surface.

Despite the evidence for physisorption, as indicated above, the presence of functional groups such as carbonyl (C=O) and hydroxyl (-OH) groups on DPAC implies the possibility of chemisorption mechanisms occurring. There is the possibility of chemical interaction between the amine groups (-NH_2) of CBZ and the carbonyl groups on DPAC, which could lead to the formation of imine bonds (C=N). This interaction would result in the release of water molecules, signifying the occurrence of chemisorption. However, the FTIR spectra indicates that these chemical changes are subtle, which may be attributed to the relatively low adsorption capacity of DPAC for CBZ (3.25 mg/g). This suggests that while chemisorption occurs, it may not be the dominant mechanism, and the adsorption process is primarily driven by physisorption. To quantify the ratio of these two mechanisms, further studies such as desorption analysis or temperature-programmed desorption (TPD) could be conducted.

3.7. Regeneration

The chemical regeneration of spent DPAC was evaluated over four cycles and the results are shown in as can be seen in Fig. S7. Solvent regeneration achieved a regeneration efficiency of 94 % after a single regeneration, and the adsorption capacity of the regenerated DPAC leveled down after four regenerations to a value of 70 % of the fresh carbon capacity and the adsorbent characteristics appeared to remain relatively intact during regeneration. The decrease in the adsorption capacity after solvent regeneration as shown in Fig. S8 is possibly due to the chemical bonding between a portion of CBZ and the DPAC surface or of "competitive adsorption" whereby methanol molecules replace CBZ on the DPAC surface. Hence, the adsorbent surface sites, occupied by methanol molecules, become unavailable for CBZ adsorption in the next adsorption cycle. It should be noted that a large proportion of the CBZ adsorbed on the DPAC surface was recovered after every methanol wash, which may indicate that the dominant mechanism in the adsorption of CBZ on DPAC is hydrophobic interaction. Fig. 9 illustrates the surface morphology of DPAC after CBZ adsorption and regeneration.

3.8. Comparison with other findings

CBZ is known for its chemical stability and recalcitrant nature, which contributes to its persistence in the environment and low removal rates in conventional water treatment processes [77]. Due to its inertness, CBZ serves as a model compound to understand the adsorption behavior of other pharmaceuticals with similar structural features. Farghal et al. [78] demonstrated that structurally related compounds such as oxcarbazepine, imipramine, and clomipramine are similarly resistant to breakdown in water and wastewater. These drugs share the same tricyclic structure as CBZ, although they differ in physicochemical properties including solubility and pKa values. As adsorption processes, these chemicals typically display π-π stacking, hydrogen bonding, and hydrophobic interactions.

A general comparison between the results obtained from this study and previous studies of BET surface area, equilibrium time, adsorptive capacity, isotherm, and kinetics models is presented in Table 6. The adsorption of CBZ onto carbonaceous adsorbents seems to be well described by both the Langmuir and the Freundlich isotherms individually or in combination in addition to Sips isotherm. This study's findings align with previous research [79–84] which consistently demonstrate that the adsorption of CBZ onto carbonaceous adsorbents is well described by both the Langmuir and Freundlich isotherms. Additionally, multiple studies reviewed confirm that the adsorption kinetics data fit best with the pseudo-second-order rate equation.

Most investigations were conducted at high concentrations of CBZ (at the mg/L scale), this study was aimed at exploring conditions high CBZ levels in addition to more representative of environmental contamination levels (μg/L range). Nevertheless, the adsorption equilibria and kinetics reported in this study agree with earlier findings. Therefore, it appears that when an isotherm or kinetic model is fitted at a certain concentration range, predictions beyond the range of experimental measurements may yield relevant results concerning the mechanisms involved in the adsorption. Extrapolation from an adsorption isotherm, obtained at high concentrations, to

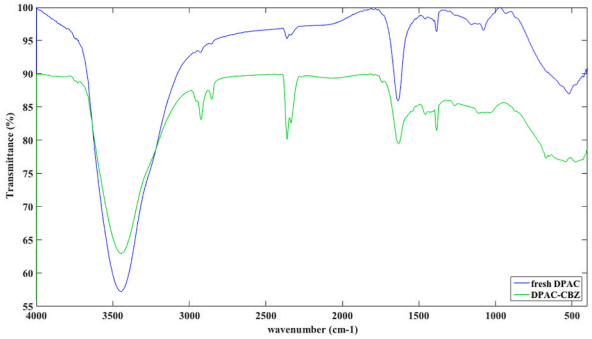

Fig. 8. FTIR spectra of DPAC before and after CBZ adsorption.

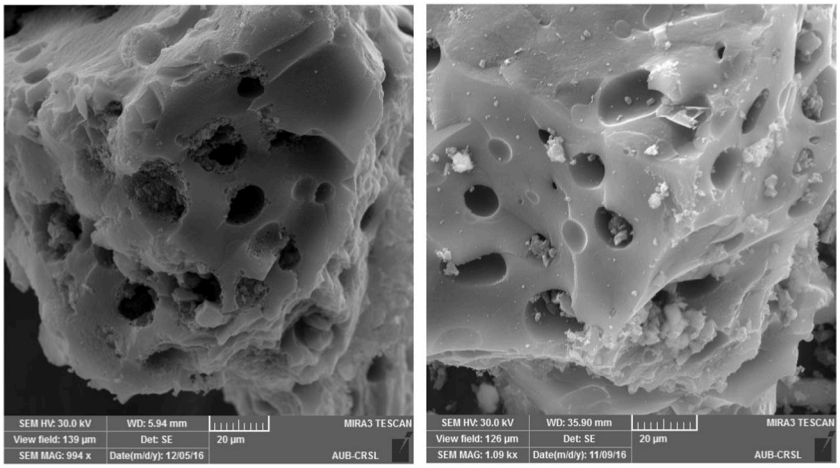

Fig. 9. SEM images of (a) CBZ saturated DPAC and (b) Regenerated DPAC.

Table 6
Comparison of BET areas, equilibrium time, adsorptive capacity, isotherm, and kinetics models for CBZ adsorption on various types of adsorbents.

Reference	Adsorbent	BET (m^2/g)	Initial CBZ conc. (mg/L)	Equilibrium time (hours)	Ads. capacity (mg/g)	Isotherm	Kinetic model
Torrellas et al. [81]	AC from peach stones	956	100	72	335	Sips	NA
Calisto et al. [79] Calisto et al. [79]	Paper mill waste	NA	5	0.083	12.6	Langmuir Freundlich	pseudo-second
Fernandez et al. [80] Fernandez et al. [80]	AC from orange peels	618	12–473	24	5.73	Langmuir	pseudo-second
Nielsen et al. [82]	AC from coconut shell	1042	1–100	NA	333	Langmuir Freundlich	NA
Shan et al. [83] Shan et al. [83]	Biochar/Fe_3O_4 from coconut shell	486	5	72	62.7	Langmuir	NA
Sotelo et al. [84]	Commercial GAC	997	1.2–2.5	360	500	Freundlich	NA
Stoykova et al. [85]	Activated Charcoal	447.1	1–20	NA	14.49	Langmuir Freundlich	NA
Yu et al. [27] [14]	Bituminous coal Flax shive	1030	6–16	NA	3.2	Freundlich	NA
This study	AC from date pits	416	0.05–0.2	8	7.22	Langmuir Freundlich	pseudo-second, pseudo first
			2–10	15			

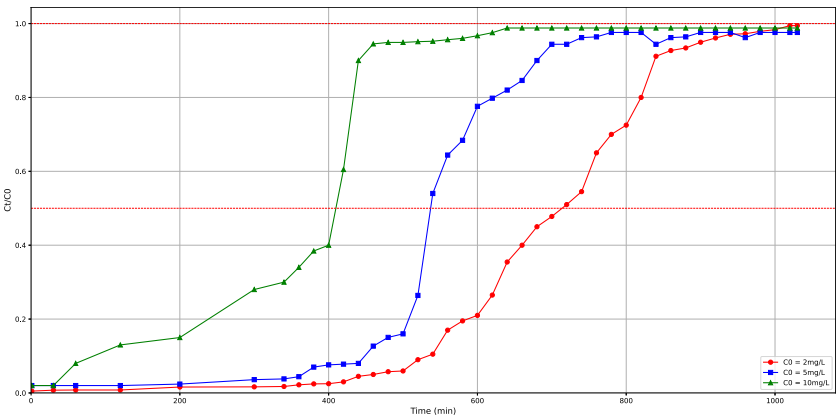

Fig. 10. Breakthrough curve for varying CBZ concentrations.

predict the capacity at a much lower concentration may lead to erroneous results and a gross overestimation of the removal capacity [27].

The adsorptive capacity achieved using DPAC was comparable to those obtained by AC prepared from orange peels, bituminous coal, and non-treated carbon prepared by paper mill pyrolysis. However, the adsorption capacity of DPAC is lower than that of Biochar/Fe_3O_4 prepared from coconut shell [83] and activated charcoal [85] despite the comparable BET surface area values. The difference in adsorptive capacity may be attributed to the presence of specific surface functional groups that would enhance the adsorption process. Finally, equilibrium using DPAC was reached after 8 h which represents a major positive characteristic since other adsorbents showed much slower kinetics. Therefore, the preparation of AC from date pits presents a potentially viable application for the removal of CBZ from aqueous solutions.

3.9. Fixed bed adsorption analysis

To study the effect of the inlet CBZ concentration on the column analysis, the concentration was taken to be 2,5, and 10 mg/L while the flow rate was chosen to be constant and fixed at 4 mL/min. The corresponding breakthrough curves at varying concentrations is shown in Fig. 10. The breakthrough curves indicate that the DPAC is consumed at a higher rate for the larger CBZ concentrations; the time for breakthrough decreases. This is due to faster saturation of binding sites in the column. Conversely, when the inlet concentration is higher, the breakthrough curve is extended which means that one can treat a larger volume of solution [86,87]. This is because lower concentrations cause slower transport due to a decrease in the diffusion coefficient and mass transfer coefficient [88].

The effect of varying flow rates was studied by repeating the experiments for a fixed concentration of CBZ of 5 mg/L with flow rates of 4, 10, and 15 mL/min. The resulting breakthrough curves shown in Fig. 11 imply that a lower flow rate allows for higher contact time thus delaying the breakthrough time. It can also be noted that there is very little difference between the 10 and 15 mL/min curves. A two-way ANOVA statistical test was used to quantify the respective effect of flow rate and inlet CBZ concentration on the breakthrough time of the columns. The variation of flow rate was evaluated to be insignificant compared to inlet CBZ concentration with 95 % confidence, i.e., p-value <0.05 and with $R^2 = 99.5$ %.

The sorption performance of the cations through the column was analyzed by the linear forms of Thomas, Yoon-Nelson, and Adams-Bohart models at concentration ratio, cut-off points set for 10 % and 97 % breakthrough ($0.1<C_t/C_o < 0.97$). Model equations, plots, and parameters are shown in Table S6. The effects of varying concentrations for a fixed flow rate and the effects of varying flow rates for a fixed concentration were investigated and the results are shown in Tables 7 and 8.

It can be seen that k_{TH} decreases as the inlet concentration of CBZ increases while q_0 increases with the increase in the inlet concentration. A high correlation with the Thomas Model indicates that internal and external diffusion processes will not be the limiting factor processes [89]. These assumptions revolve around the fact that the process follows pseudo-second-order reversible kinetics and the Langmuir isotherm. This also assumes that external and internal diffusion resistance can be neglected during the reaction processes [90]. As for the Adams-Bohart Model (ABM), the trends observed for k_{AB} and N_o are comparable to the behavior of k_{TH} and q_0 for the Thomas model. As the inlet concentration of CBZ increases, the values of k_{AB} decrease while the values of N_o increase. ABM is usually used to quantify the correlation between the data and the model at the early stages of the breakthrough curve. From these results it may be concluded that the external mass transfer rate is dominant in the system's kinetics. The assumptions that were used by Adams and Bohart are that the equilibrium of the reaction is not reached instantaneously and that the adsorption capacity of the AC and the adsorption rate of the reaction are proportional [90]. The Yoon-Nelson Model shows completely different trends. Both R^2 and τ increase as the inlet concentration of CBZ increases while the values of N_0 show an opposite trend. The overall highest value of R^2 for the experiment was 0.9875 for the Yoon-Nelson Model at an inlet concentration of CBZ of 2 mg/L.

As for the variable flow experiment, the results are somewhat contradictory. The Thomas Model, shows an increase in the k_{TH} values with increased flow rate but then the k_{TH} values decrease when the inlet flow rate increases beyond 10 mL/min. The values of q_0 and R^2 showed the opposite trend; they decreased at the beginning and then increased again when the inlet flow surpassed 10 mL/min. AS for the ABM model, the value of k_{AB} decreased when the inlet flow was increased from 4 to 10 mL/min and then increased again when the inlet flow reached 15 mL/min; the values of R^2 followed an increasing pattern before showing a plateau when the inlet flow reached 15 mL/min. Finally, for the YNM model, the values of k_{YN} peaked when the inlet flow reached 10 mL/min; τ followed a decreasing trend and R^2 followed an increasing trend. The overall highest value of R^2 for the experiment was 0.9778 for the Adams-Bohart Model at a flow rate of 10 and 15 mL/min.

4. Conclusion

This study demonstrated the effectiveness of DPAC in removing CBZ from water. The generated DPAC demonstrated a specific surface area of 309 m^2/g, a pore volume of 0.264 cm^3/g, and the pores are mainly distributed at 1.86, 2.73, and 3.43 nm. The effects of pH and temperature were significant, with the validation of Langmuir, Freundlich, Sips, and Toth isotherms showing monolayer adsorption and heterogeneous surface conditions. The experimental data were fitted to several theoretical models, such as the Thomas Model, the Bohart-Adams Model, and the Yoon-Nelson Model. Quantitative analysis suggests that adsorption is partially controlled by intra-particle diffusion and may also be determined by the surface chemistry of the adsorbent. The LDF model proved to be a valuable tool for elucidating CBZ adsorption kinetics onto DPAC. However, the model performance was influenced mostly by initial adsorbate concentration and to a lesser extent by acidic pH levels. Thermodynamic analysis revealed the adsorption process to be endothermic, spontaneous, and entropically driven, significantly impacted by temperature and adsorbate concentration. The regeneration of the spent DPAC was carried out using methanol and the regenerated adsorbent was used for four regeneration cycles and showed a

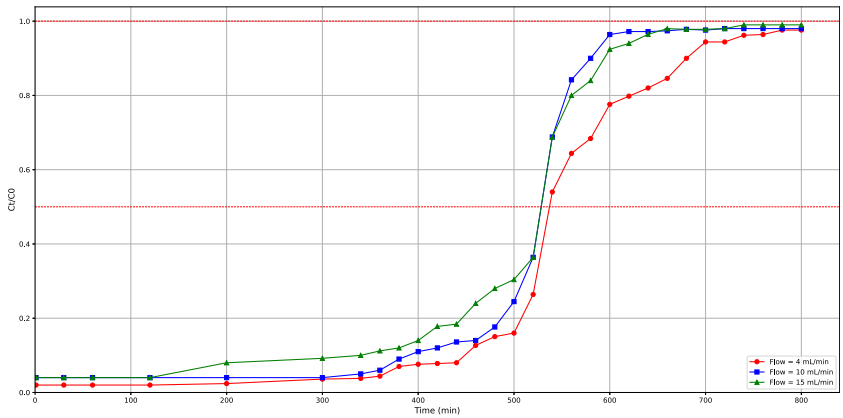

Fig. 11. Breakthrough curves for varying inlet flowrate.

Table 7
Adsorption parameters for different models with varying CBZ concentration with a fixed inlet flow rate of 4 mL/min.

Column adsorption model	**Model parameter**	Inlet CBZ concentration (mg/L)		
		2	**5**	**10**
Thomas	k_{TH} (L/min.mg)	5.251E-03	2.207E-03	1.318E-03
	q_0 (mg/g)	76.30	150.93	183.04
	R^2	0.9328	0.9747	0.883
ABM	k_{AB} (mL/min.mg)	−3.198E-03	−3.050E-03	−1.445E-03
	N_o (mg/L)	287	437	470
	R^2	0.9565	0.9745	0.8449
YNM	k_{YN} (L/min)	1.081E-02	1.273E-02	1.312E-02
	τ (min)	683	536	324
	R^2	0.9875	0.9213	0.8231

Table 8
Adsorption parameters for different models with varying inlet flow with fixed inlet CBZ concentration of 5 mg/L.

Column adsorption model	**Model parameter**	Inlet flow (mL/min)		
		4	**10**	**15**
Thomas	k_{TH} (L/min.mg)	2.207E-03	2.363E-03	2.056E-03
	q_0 (mg/g)	150.93	130.95	131.59
	R^2	0.9747	0.928	0.9588
ABM	k_{AB} (mL/min.mg)	−3.050E-03	−3.362E-03	−3.198E-03
	N_o (mg/L)	437	998	1445
	R^2	0.9213	0.9778	0.9778
YNM	k_{YN} (L/min)	1.273E-02	1.378E-02	1.229E-02
	τ (min)	536	477	469
	R^2	0.9213	0.9230	0.9588

regeneration efficiency of 94 % on the first iteration and then dropped to 70 % after the fourth iteration. Future research should focus on optimizing activation processes and exploring DPAC's effectiveness for other contaminants, contributing to the development of cost-effective and environmentally friendly water treatment technologies. Customizing and optimizing adsorption settings based on the unique properties of the adsorbate and the chemistry of the solution is crucial for enhancing the efficiency of pharmaceutical contaminant removal from wastewater using DPAC. The application of activated carbon produced from biomass for wastewater and water treatment is not a new topic since their use in this field is well established. However, with continuous development and research, the treatment evolved. While this study shows that DPAC is effective in removing CBZ, there are some important limitations that should be highlighted. To fully comprehend the adsorption mechanism, particularly the equilibrium between chemisorption and physisorption, more research is required. Moreover, a four-cycle fall in efficiency followed DPAC's short-term remarkable regeneration potential, highlighting the need for optimized regeneration processes. Future research should examine the consequences of competitive adsorption in more complex water matrices, where additional contaminants may reduce DPAC's adsorption ability. It is also important to assess the scalability of DPAC in larger water treatment systems, ensuring its efficiency and cost-effectiveness when applied at an industrial or municipal scale.

CRediT authorship contribution statement

Ramez M. Zayyat: Writing – review & editing, Writing – original draft, Software, Methodology, Formal analysis. **Rim Yahfoufi:** Writing – original draft, Methodology, Conceptualization. **Mahmoud Al-Hindi:** Writing – review & editing, Supervision, Investigation, Funding acquisition, Formal analysis. **Michel A. Kordahi:** Writing – original draft, Software. **George M. Ayoub:** Writing – review & editing. **Mohammad N. Ahmad:** Writing – review & editing.

Competing interests

The authors have no relevant financial or non-financial interests to disclose.

Data availability statement

The processed data required to reproduce the above findings are available to download from: https://github.com/Ramezzayyat/Elucidating-the-Dynamics-of-Carbamazepine-Uptake-

Funding

The authors would like to acknowledge the financial support received from the University Research Board (Award# 103371; Project# 23279) of the American University of Beirut.

Declaration of competing interest

The authors declare that they have no known competing financial interests or personal relationships that could have appeared to influence the work reported in this paper.

Appendix A. Supplementary data

Supplementary data to this article can be found online at https://doi.org/10.1016/j.heliyon.2024.e39068.

References

[1] A. Almeida, A. Soares, V.I. Esteves, R. Freitas, Occurrence of the antiepileptic carbamazepine in water and bivalves from marine environments: a review, Environ. Toxicol. Pharmacol. 86 (Aug 2021) 103661, https://doi.org/10.1016/j.etap.2021.103661.
[2] N. Mheidli, A. Malli, F. Mansour, M. Al-Hindi, Occurrence and risk assessment of pharmaceuticals in surface waters of the Middle East and North Africa: a review, Sci. Total Environ. 851 (2022/12/10/2022) 158302, https://doi.org/10.1016/j.scitotenv.2022.158302.
[3] L.A.A. Freitas, G. Radis-Baptista, Pharmaceutical pollution and disposal of expired, unused, and unwanted medicines in the Brazilian context, J Xenobiot 11 (2) (May 18 2021) 61–76, https://doi.org/10.3390/jox11020005.
[4] F. Mansour, M. Al-Hindi, W. Saad, D. Salam, Environmental risk analysis and prioritization of pharmaceuticals in a developing world context, Sci. Total Environ. 557–558 (Jul 1 2016) 31–43, https://doi.org/10.1016/j.scitotenv.2016.03.023.
[5] M. Patel, R. Kumar, K. Kishor, T. Mlsna, C.U. Pittman Jr., D. Mohan, Pharmaceuticals of emerging concern in aquatic systems: chemistry, occurrence, effects, and removal methods, Chem. Rev. 119 (6) (Mar 27 2019) 3510–3673, https://doi.org/10.1021/acs.chemrev.8b00299.
[6] M. Kahle, I.J. Buerge, M.D. Müller, T. Poiger, Hydrophilic anthropogenic markers for quantification of wastewater contamination in ground- and surface waters, Environ. Toxicol. Chem. 28 (12) (Dec 2009) 2528–2536, https://doi.org/10.1897/08-606.1 (in eng).
[7] A.J. Wicht, K. Heye, A. Schmidt, J. Oehlmann, C. Huhn, The wastewater micropollutant carbamazepine in insectivorous birds-an exposure estimate, Anal. Bioanal. Chem. 414 (17) (Jul 2022) 4909–4917, https://doi.org/10.1007/s00216-022-04117-0.
[8] J. Xiang, M. Wu, J. Lei, C. Fu, J. Gu, G. Xu, The fate and risk assessment of psychiatric pharmaceuticals from psychiatric hospital effluent, Ecotoxicol. Environ. Saf. 150 (Apr 15 2018) 289–296, https://doi.org/10.1016/j.ecoenv.2017.12.049.
[9] Â. Almeida, et al., Presence of the pharmaceutical drug carbamazepine in coastal systems: effects on bivalves, Aquat. Toxicol. 156 (2014/11/01/2014) 74–87, https://doi.org/10.1016/j.aquatox.2014.08.002.
[10] M. Verma, Review of advanced oxidation processes (AOPs) for treatment of pharmaceutical wastewater, koreascience.or.kr (2020), https://doi.org/10.12989/aer.2020.9.1.001.
[11] L. Dirani, G.M. Ayoub, L. Malaeb, R.M. Zayyat, A review on the occurrence of per- and polyfluoroalkyl substances in the aquatic environment and treatment trends for their removal, J. Environ. Chem. Eng. 12 (5) (Oct 2024) 113325, https://doi.org/10.1016/j.jece.2024.113325. ARTN 113325.
[12] H. Zeghioud, L. Fryda, H. Djelal, A. Assadi, A. Kane, A comprehensive review of biochar in removal of organic pollutants from wastewater: characterization, toxicity, activation/functionalization and influencing treatment factors, J. Water Proc. Eng. 47 (2022), https://doi.org/10.1016/j.jwpe.2022.102801.
[13] F. Mansour, M. Al-Hindi, R. Yahfoufi, G.M. Ayoub, M.N. Ahmad, The use of activated carbon for the removal of pharmaceuticals from aqueous solutions: a review, Rev. Environ. Sci. Biotechnol. 17 (1) (2017) 109–145, https://doi.org/10.1007/s11157-017-9456-8.
[14] A. Aghababaei, V.B. Borugadda, A. Dalai, C.H. Niu, An investigation on adsorption of carbamazepine with adsorbents developed from flax shives: kinetics, mechanisms, and desorption, Chem. Eng. Res. Des. 189 (2023/01/01/2023) 138–155, https://doi.org/10.1016/j.cherd.2022.11.008.
[15] G. Özçelik, M. Bilgin, S. Şahin, Carbamazepine sorption characteristics onto bentonite clay: box-Behnken process design, Sustainable Chemistry and Pharmacy 18 (2020), https://doi.org/10.1016/j.scp.2020.100323.
[16] M. Fischer, Adsorption of carbamazepine in all-silica zeolites studied with density functional theory calculations, ChemPhysChem 24 (9) (May 2 2023) e202300022, https://doi.org/10.1002/cphc.202300022.
[17] S. Ravi, Y. Choi, J.K. Choe, Novel phenyl-phosphate-based porous organic polymers for removal of pharmaceutical contaminants in water, Chem. Eng. J. 379 (2020), https://doi.org/10.1016/j.cej.2019.122290.

[18] M.A. Décima, S. Marzeddu, M. Barchiesi, C. Di Marcantonio, A. Chiavola, M.R. Boni, A review on the removal of carbamazepine from aqueous solution by using activated carbon and biochar, Sustainability 13 (21) (2021), https://doi.org/10.3390/su132111760.

[19] G. Liang, Z. Hu, Z. Wang, X. Yang, X. Xie, J. Zhao, Effective removal of carbamazepine and diclofenac by CuO/Cu(2)O/Cu-biochar composite with different adsorption mechanisms, Environ. Sci. Pollut. Res. Int. 27 (36) (Dec 2020) 45435–45446, https://doi.org/10.1007/s11356-020-10284-3.

[20] M.J. Ahmed, Preparation of activated carbons from date (Phoenix dactylifera L.) palm stones and application for wastewater treatments: review, Process Saf. Environ. Protect. 102 (2016) 168–182, https://doi.org/10.1016/j.psep.2016.03.010.

[21] M. Naghdi, et al., Pine-wood derived nanobiochar for removal of carbamazepine from aqueous media: adsorption behavior and influential parameters, Arab. J. Chem. 12 (8) (2019/12/01/2019) 5292–5301, https://doi.org/10.1016/j.arabjc.2016.12.025.

[22] V. Vinayagam, et al., Sustainable adsorbents for the removal of pharmaceuticals from wastewater: a review, Chemosphere 300 (Aug 2022) 134597, https://doi.org/10.1016/j.chemosphere.2022.134597.

[23] L. Nielsen, P. Zhang, T.J. Bandosz, Adsorption of carbamazepine on sludge/fish waste derived adsorbents: effect of surface chemistry and texture, Chem. Eng. J. 267 (2015) 170–181, https://doi.org/10.1016/j.cej.2014.12.113.

[24] X. Li, F.I. Hai, L.D. Nghiem, Simultaneous activated carbon adsorption within a membrane bioreactor for an enhanced micropollutant removal, Bioresour. Technol. 102 (9) (May 2011) 5319–5324, https://doi.org/10.1016/j.biortech.2010.11.070.

[25] M. Ek, C. Baresel, J. Magner, R. Bergstrom, M. Harding, Activated carbon for the removal of pharmaceutical residues from treated wastewater, Water Sci. Technol. 69 (11) (2014) 2372–2380, https://doi.org/10.2166/wst.2014.172.

[26] T.X. Bui, H. Choi, Adsorptive removal of selected pharmaceuticals by mesoporous silica SBA-15, J. Hazard Mater. 168 (2–3) (Sep 15 2009) 602–608, https://doi.org/10.1016/j.jhazmat.2009.02.072.

[27] Z. Yu, S. Peldszus, P.M. Huck, Adsorption characteristics of selected pharmaceuticals and an endocrine disrupting compound-Naproxen, carbamazepine and nonylphenol-on activated carbon, Water Res. 42 (12) (Jun 2008) 2873–2882, https://doi.org/10.1016/j.watres.2008.02.020.

[28] D. Shan, S. Deng, T. Zhao, G. Yu, J. Winglee, M.R. Wiesner, Preparation of regenerable granular carbon nanotubes by a simple heating-filtration method for efficient removal of typical pharmaceuticals, Chem. Eng. J. 294 (2016) 353–361, https://doi.org/10.1016/j.cej.2016.02.118.

[29] H. Fallou, N. Cimetiere, S. Giraudet, D. Wolbert, P. Le Cloirec, Adsorption of pharmaceuticals onto activated carbon fiber cloths - modeling and extrapolation of adsorption isotherms at very low concentrations, J. Environ. Manag. 166 (Jan 15 2016) 544–555, https://doi.org/10.1016/j.jenvman.2015.10.056.

[30] N. Suriyanon, P. Punyapalakul, C. Ngamcharussrivichai, Mechanistic study of diclofenac and carbamazepine adsorption on functionalized silica-based porous materials, Chem. Eng. J. 214 (2013) 208–218, https://doi.org/10.1016/j.cej.2012.10.052.

[31] C.M. Dai, S.U. Geissen, Y.L. Zhang, Y.J. Zhang, X.F. Zhou, Performance evaluation and application of molecularly imprinted polymer for separation of carbamazepine in aqueous solution, J. Hazard Mater. 184 (1–3) (Dec 15 2010) 156–163, https://doi.org/10.1016/j.jhazmat.2010.08.018.

[32] M. Baghdadi, E. Ghaffari, B. Aminzadeh, Removal of carbamazepine from municipal wastewater effluent using optimally synthesized magnetic activated carbon: adsorption and sedimentation kinetic studies, J. Environ. Chem. Eng. 4 (3) (2016) 3309–3321, https://doi.org/10.1016/j.jece.2016.06.034.

[33] J.R. Domínguez-Vargas, T. Gonzalez, P. Palo, E.M. Cuerda-Correa, Removal of carbamazepine, naproxen, and trimethoprim from water by amberlite XAD-7: a kinetic study, Clean: Soil, Air, Water 41 (11) (2013) 1052–1061, https://doi.org/10.1002/clen.201200245.

[34] J.A.-S. Marjan Alaghmand, Sabrina Barkat, Adsorption and removal of a selected emerging contaminant, carbamazepine, using Humic acid, Humasorb and Montmorillonite. Equilibrium isotherms, kinetics and effect of the water matrix, Journal of Environmental Science and Health, Part A (2020), https://doi.org/10.12989/aer.2020.9.1.001.

[35] C.A. Adeyanju, et al., Recent advances on the aqueous phase adsorption of carbamazepine, ChemBioEng Rev. 9 (3) (2022) 231–247, https://doi.org/10.1002/cben.202100042.

[36] S. Mondal, S. Patel, S.K. Majumder, Naproxen removal capacity enhancement by transforming the activated carbon into a blended composite material, Water, Air, Soil Pollut. 231 (2) (2020), https://doi.org/10.1007/s11270-020-4411-7.

[37] A. Aldeguer Esquerdo, P.J. Varo Galvan, I. Sentana Gadea, D. Prats Rico, Carbamazepine and diclofenac removal double treatment: oxidation and adsorption, Int. J. Environ. Res. Publ. Health 18 (13) (Jul 4 2021), https://doi.org/10.3390/ijerph18137163.

[38] B. Vojnović, M. Cetina, P. Franjković, A. Sutlović, Influence of initial pH value on the adsorption of reactive black 5 dye on powdered activated carbon: kinetics, mechanisms, and thermodynamics, Molecules 27 (4) (Feb 16 2022), https://doi.org/10.3390/molecules27041349 (in eng).

[39] M. Kilic, E. Apaydin-Varol, A.E. Pütün, Adsorptive removal of phenol from aqueous solutions on activated carbon prepared from tobacco residues: equilibrium, kinetics and thermodynamics, J. Hazard Mater. 189 (1) (2011/05/15/2011) 397–403, https://doi.org/10.1016/j.jhazmat.2011.02.051.

[40] A.L. Cazetta, et al., NaOH-activated carbon of high surface area produced from coconut shell: kinetics and equilibrium studies from the methylene blue adsorption, Chem. Eng. J. 174 (1) (2011/10/15/2011) 117–125, https://doi.org/10.1016/j.cej.2011.08.058.

[41] E.M. Chatir, A. El Hadrami, S. Ojala, R. Brahmi, Production of activated carbon with tunable porosity and surface chemistry via chemical activation of hydrochar with phosphoric acid under oxidizing atmosphere, Surface. Interfac. 30 (2022/06/01/2022) 101849, https://doi.org/10.1016/j.surfin.2022.101849.

[42] S. Hazourli, M. Ziati, A. Hazourli, Characterization of activated carbon prepared from lignocellulosic natural residue:-Example of date stones, Phys. Procedia 2 (3) (2009/11/01/2009) 1039–1043, https://doi.org/10.1016/j.phpro.2009.11.060.

[43] Z. Qie, et al., Effect of pretreatment and activation conditions on pore development of coal-based activated carbon, J. Ind. Eng. Chem. (2024), https://doi.org/10.1016/j.jiec.2024.05.037, 2024/05/21.

[44] H. Yang, J. Liu, B. Pang, J. Chi, Effect of different pretreatment methods on pore structure of activated carbon, J. Phys. Conf. 1774 (1) (2021/01/01 2021) 012067, https://doi.org/10.1088/1742-6596/1774/1/012067.

[45] X. Jin, et al., Nitrogen and sulfur Co-doped hierarchically porous carbon nanotubes for fast potassium ion storage, Small 18 (42) (2022) 2203545, https://doi.org/10.1002/smll.202203545.

[46] J. Yang, et al., Engineering a hollow bowl-like porous carbon-confined Ru–MgO hetero-structured nanopair as a high-performance catalyst for ammonia borane hydrolysis, Mater. Horiz. 11 (8) (2024) 2032–2040, https://doi.org/10.1039/D3MH01909H, 10.1039/D3MH01909H.

[47] T.V. Madureira, M.J. Rocha, Q.B. Cass, M.E. Tiritan, Development and optimization of a HPLC-DAD method for the determination of diverse pharmaceuticals in estuarine surface waters, J. Chromatogr. Sci. 48 (3) (Mar 2010) 176–182, https://doi.org/10.1093/chromsci/48.3.176 (in eng).

[48] H.A. Mowafy, F.K. Alanazi, G.M. El Maghraby, Development and validation of an HPLC-UV method for the quantification of carbamazepine in rabbit plasma, Saudi Pharmaceut. J. 20 (1) (Jan 2012) 29–34, https://doi.org/10.1016/j.jsps.2011.04.003 (in eng).

[49] E. Ezzeldin, A. Shahat, O. Basudan, Development and validation of an HPLC method for the determination of carbamazepine in human plasma, Life Sci. J. 10 (2013) 2159–2163.

[50] S. Feijoo, M. Kamali, R. Dewil, A review of wastewater treatment technologies for the degradation of pharmaceutically active compounds: carbamazepine as a case study, Chem. Eng. J. 455 (2023/01/01/2023) 140589, https://doi.org/10.1016/j.cej.2022.140589.

[51] M. Yao, L. Duan, J. Wei, F. Qian, S.W. Hermanowicz, Carbamazepine removal from wastewater and the degradation mechanism in a submerged forward osmotic membrane bioreactor, Bioresour. Technol. 314 (Oct 2020) 123732, https://doi.org/10.1016/j.biortech.2020.123732.

[52] Y. Zhang, S.U. Geissen, Prediction of carbamazepine in sewage treatment plant effluents and its implications for control strategies of pharmaceutical aquatic contamination, Chemosphere 80 (11) (Sep 2010) 1345–1352, https://doi.org/10.1016/j.chemosphere.2010.06.030.

[53] K.Y. Foo, B.H. Hameed, Insights into the modeling of adsorption isotherm systems, Chem. Eng. J. 156 (1) (2010) 2–10, https://doi.org/10.1016/j.cej.2009.09.013.

[54] Positteam, RStudio: Integrated Development Environment for R, 2024.

[55] K.S.K. Reddy, A. Al Shoaibi, C. Srinivasakannan, A comparison of microstructure and adsorption characteristics of activated carbons by CO2 and H3PO4 activation from date palm pits, N. Carbon Mater. 27 (5) (2012 2012) 344–351, https://doi.org/10.1016/s1872-5805(12)60020-1.

[56] M.A. Al-Ghouti, Z.A. Al Disi, N. Al-Kaabi, M. Khraisheh, Mechanistic insights into the remediation of bromide ions from desalinated water using roasted date pits, Chem. Eng. J. 308 (2017) 463–475, https://doi.org/10.1016/j.cej.2016.09.091.

[57] F. Al-Qaessi, L. Abu-Farah, Activated carbon production from date stones using phosphoric acid, Energy Sources, Part A Recovery, Util. Environ. Eff. 32 (14) (2010) 1316–1325, https://doi.org/10.1080/15567030802654012.
[58] M. Kim, et al., KOH-activated hollow ZIF-8 derived porous carbon: nanoarchitectured control for upgraded capacitive deionization and supercapacitor, ACS Appl. Mater. Interfaces 13 (44) (Nov 10 2021) 52034–52043, https://doi.org/10.1021/acsami.1c09107 (in eng).
[59] R. Farma, Physical properties analysis of activated carbon from oil palm empty fruit bunch fiber on methylene blue adsorption, Journal of Technomaterials Physics 1 (2019) 67–73, https://doi.org/10.32734/jotp.v1i1.824, 02/28.
[60] S.-M. Lee, S.-H. Lee, J.-S. Roh, Analysis of activation process of carbon black based on structural parameters obtained by XRD analysis, Crystals 11 (2) (2021) 153 [Online]. Available: https://www.mdpi.com/2073-4352/11/2/153.
[61] M.A. Décima, S. Marzeddu, M. Barchiesi, C. Di Marcantonio, A. Chiavola, M.R. Boni, A review on the removal of carbamazepine from aqueous solution by using activated carbon and biochar, Sustainability 13 (21) (2021) 11760 [Online]. Available: https://www.mdpi.com/2071-1050/13/21/11760.
[62] F. Amalina, A.S.A. Razak, S. Krishnan, H. Sulaiman, A.W. Zularisam, M. Nasrullah, Biochar production techniques utilizing biomass waste-derived materials and environmental applications – a review, Journal of Hazardous Materials Advances 7 (2022) 100134, https://doi.org/10.1016/j.hazadv.2022.100134, 2022/08/01/.
[63] R.M.A. Viegas, et al., Carbamazepine adsorption with a series of organoclays: removal and toxicity analyses, Appl. Water Sci. 14 (6) (2024) 133, https://doi.org/10.1007/s13201-024-02198-z, 2024/05/13.
[64] L.F. Delgado, P. Charles, K. Glucina, C. Morlay, Adsorption of ibuprofen and atenolol at trace concentration on activated carbon, Separ. Sci. Technol. 50 (10) (2014) 1487–1496, https://doi.org/10.1080/01496395.2014.975360.
[65] A.E. Rodrigues, C.M. Silva, What's wrong with Lagergreen pseudo first order model for adsorption kinetics? Chem. Eng. J. 306 (2016) 1138–1142, https://doi.org/10.1016/j.cej.2016.08.055, 2016/12/15/.
[66] S.P.D. Monte Blanco, et al., Kinetic, equilibrium and thermodynamic phenomenological modeling of reactive dye adsorption onto polymeric adsorbent, Chem. Eng. J. 307 (2017) 466–475, https://doi.org/10.1016/j.cej.2016.08.104, 2017/01/01/.
[67] L. Largitte, R. Pasquier, New models for kinetics and equilibrium homogeneous adsorption, Chem. Eng. Res. Des. 112 (2016) 289–297, https://doi.org/10.1016/j.cherd.2016.06.021, 2016/08/01/.
[68] M.J. Rupa, A. Pal, S. Mitra, B.B. Saha, Time adapted linear driving force model for gas adsorption onto solids, Chem. Eng. J. 420 (2021) 129785, https://doi.org/10.1016/j.cej.2021.129785, 2021/09/15/.
[69] J. Hills, An investigation of the linear driving force approximation to diffusion in spherical particles, Chem. Eng. Sci. 41 (11) (1986) 2779–2785.
[70] S. Sircar, J.R. Hufton, Intraparticle adsorbate concentration profile for linear driving force model, American Institute of Chemical Engineers. AIChE Journal 46 (3) (2000) 659 (in English), https://www.proquest.com/scholarly-journals/intraparticle-adsorbate-concentration-profile/docview/199384371/se-2?accountid=8555. Sircar%2C+S%3BHufton%2C+J+R&issn=00011541&title=American+Institute+of+Chemical+Engineers.+AIChE+Journal&volume=46&issue=3&date=2000-03-01&spage=659&id=doi:&sid=ProQ_ss&genre=article.
[71] S. Sircar, J.R. Hufton, Why does the linear driving force model for adsorption kinetics work? Adsorption 6 (2) (2004) 137–147.
[72] I. Anastopoulos, G.Z. Kyzas, Are the thermodynamic parameters correctly estimated in liquid-phase adsorption phenomena? J. Mol. Liq. 218 (2016) 174–185, https://doi.org/10.1016/j.molliq.2016.02.059.
[73] P. Saha, S. Chowdhury, in: P.M.T. Thermodynamics (Ed.), Insight into Adsorption Thermodynamics, InTech, 2011 ch. (Chapter 16).
[74] M. Sarkar, P.K. Acharya, B. Bhattacharya, Modeling the adsorption kinetics of some priority organic pollutants in water from diffusion and activation energy parameters, J. Colloid Interface Sci. 266 (1) (Oct 1 2003) 28–32, https://doi.org/10.1016/s0021-9797(03)00551-4.
[75] W.J. Weber, J.C. Morris, Kinetics of adsorption on carbon from solution, J. Sanit. Eng. Div. 89 (2) (1963) 31–60.
[76] F.-C. Wu, R.-L. Tseng, R.-S. Juang, Initial behavior of intraparticle diffusion model used in the description of adsorption kinetics, Chem. Eng. J. 153 (1) (2009/11/01/2009) 1–8, https://doi.org/10.1016/j.cej.2009.04.042.
[77] C. Ji, J. Hou, K. Wang, Y. Zhang, V. Chen, Biocatalytic degradation of carbamazepine with immobilized laccase-mediator membrane hybrid reactor, J. Membr. Sci. 502 (2016/03/15/2016) 11–20, https://doi.org/10.1016/j.memsci.2015.12.043.
[78] H.H. Farghal, M. Nebsen, L. Blaney, M.M.H. El-Sayed, Treatment of carbamazepine and other structurally-related pharmaceuticals in water and wastewater by nanoporous adsorbents and photocatalysts: a critical review, Rev. Chem. Eng. 40 (5) (2024) 641–665, https://doi.org/10.1515/revce-2023-0038.
[79] V. Calisto, C.I. Ferreira, J.A. Oliveira, M. Otero, V.I. Esteves, Adsorptive removal of pharmaceuticals from water by commercial and waste-based carbons, J. Environ. Manag. 152 (Apr 1 2015) 83–90, https://doi.org/10.1016/j.jenvman.2015.01.019.
[80] M.E. Fernandez, B. Ledesma, S. Roman, P.R. Bonelli, A.L. Cukierman, Development and characterization of activated hydrochars from orange peels as potential adsorbents for emerging organic contaminants, Bioresour. Technol. 183 (May 2015) 221–228, https://doi.org/10.1016/j.biortech.2015.02.035.
[81] S.Á. Torrellas, R. García Lovera, N. Escalona, C. Sepúlveda, J.L. Sotelo, J. García, Chemical-activated carbons from peach stones for the adsorption of emerging contaminants in aqueous solutions, Chem. Eng. J. 279 (2015) 788–798, https://doi.org/10.1016/j.cej.2015.05.104.
[82] L. Nielsen, M.J. Biggs, W. Skinner, T.J. Bandosz, The effects of activated carbon surface features on the reactive adsorption of carbamazepine and sulfamethoxazole, Carbon 80 (2014) 419–432, https://doi.org/10.1016/j.carbon.2014.08.081.
[83] D. Shan, et al., Preparation of ultrafine magnetic biochar and activated carbon for pharmaceutical adsorption and subsequent degradation by ball milling, J. Hazard Mater. 305 (Mar 15 2016) 156–163, https://doi.org/10.1016/j.jhazmat.2015.11.047.
[84] J.L. Sotelo, G. Ovejero, A. Rodríguez, S. Álvarez, J. García, Adsorption of carbamazepine in fixed bed columns: experimental and modeling studies, Separ. Sci. Technol. 48 (17) (2013) 2626–2637, https://doi.org/10.1080/01496395.2013.808215.
[85] M. Stoykova, B. Koumanova, L. Morl, Adsorptive removal of carbmazepine from wastewaters by activated charcoals, Journal of Chemical Technology and Metallurgy 48 (5) (2013) 469–474.
[86] I.A.W. Tan, A.L. Ahmad, B.H. Hameed, Adsorption of basic dye using activated carbon prepared from oil palm shell: batch and fixed bed studies, Desalination 225 (1–3) (2008/05/01/2008) 13–28, https://doi.org/10.1016/j.desal.2007.07.005.
[87] A.A. Ahmad, B.H. Hameed, Fixed-bed adsorption of reactive azo dye onto granular activated carbon prepared from waste, J. Hazard Mater. 175 (1–3) (Mar 15 2010) 298–303, https://doi.org/10.1016/j.jhazmat.2009.10.003.
[88] R.M. Zayyat, M.T. Suidan, Attenuation of 17α-ethynylestradiol onto model vegetable waste, Clean Technol. Environ. Policy 20 (2018) 2275–2286.
[89] Z.Z. Chowdhury, S.M. Zain, A.K. Rashid, R.F. Rafique, K. Khalid, Breakthrough curve analysis for column dynamics sorption of Mn(II) ions from wastewater by UsingMangostana garciniaPeel-based granular-activated carbon, J. Chem. 2013 (2013) 1–8, https://doi.org/10.1155/2013/959761.
[90] O. Długosz, M. Banach, Sorption of Ag+ and Cu2+ by vermiculite in a fixed-bed column: design, process optimization and dynamics investigations, Appl. Sci. 8 (11) (2018) 2221, https://doi.org/10.3390/app8112221.